EXPERIMENTAL TESTS OF QUANTUM ELECTRODYNAMICS

AND

SPECTRAL REPRESENTATIONS OF GREEN'S FUNCTIONS

IN PERTURBATION THEORY

A DISSERTATION

SUBMITTED TO THE DEPARTMENT OF PHYSICS

AND THE COMMITTEE ON GRADUATE STUDY

OF STANFORD UNIVERSITY

IN PARTIAL FULFILLMENT OF THE REQUIREMENTS

FOR THE DEGREE OF

DOCTOR OF PHILOSOPHY

By

James Daniel Bjorken

April 1959

I certify that I have read this thesis and that in my opinion it is fully adequate, in scope and quality, as a dissertation for the degree of Doctor of Philosophy.

Sidney Drell

I certify that I have read this thesis and that in my opinion it is fully adequate, in scope and quality, as a dissertation for the degree of Doctor of Philosophy.

Marshall Baker

Approved for the University Committee on Graduate Study:

Albert H. Bowker
Dean of the Graduate Division

ACKNOWLEDGMENTS

It is a pleasure to thank Professor Sidney Drell for the great deal of instruction, advice, and encouragement over the past years. His suggestions have greatly implemented the completion of this work.

The author would also like to thank Dr. Marshall Baker for the helpful criticism of the second half of this thesis.

Helpful conversations with Dr. Burton Richter, Professor W. K. H. Panofsky, and Dr. S. Mandelstam are gratefully acknowledged.

Financial support has been provided by the National Science Foundation.

TABLE OF CONTENTS

LIST OF ILLUSTRATIONS

EXPERIMENTAL TESTS OF QUANTUM ELECTRODYNAMICS*

I. INTRODUCTION

Although at present quantum electrodynamics has met every experimental challenge, there are still strong theoretical misgivings concerning its internal consistency.[1] The divergences, inherited from the classical difficulties associated with the notion of point particle, indicate that the idea of point particle and point interaction as used in quantum electrodynamics may be incorrect, and that unknown structure effects may appear at small distances.

A possible breakdown in quantum electrodynamics might manifest itself in any of the following ways: the photon might have a finite size, i.e., the photon propagator might contain a form factor which is not accounted for in the present theory; or the electron might have a finite size, manifested in form factors in either the vertex operator or the propagator or both, as related by gauge invariance.[2] Additional evidence regarding

---

*Submitted with S. D. Drell for publication in the Physical Review.

[1] R. P. Feynman, Acad. Brasil de Cienc. 26, 51 (1954)

[2] S. D. Drell, Annals of Physics 4, No. 1, 75 (1958)

the validity of quantum electrodynamics as applied to μ-mesons might be found in a study of the structure of the μ-meson. In fact, the validity of the assumption that the μ-meson is a "heavy electron" can be tested by comparing two different experiments, in one of which electrons undergo the same interactions as do μ-mesons in the other. Evidence of a difference in their structure might then serve as a strongly desired first clue to the problem of understanding what it is that is responsible for their large mass difference.

By size of a particle is meant here merely a convenient measure of the limits of the present theory of quantum electrodynamics. We shall follow the conventions in reference 2, where for propagators "size" meant the length $1/\Lambda$, corresponding to the regulator mass Λ introduced into the propagators ($\hbar = c = 1$). We shall also use the same convention here for the vertex. In this way we associate a size with the electron or μ-meson vertex according to the expansion $F_V(q^2) = 1 + q_\mu q^\mu d^2$; hence the distance d is smaller by $(1/6)^{\frac{1}{2}}$ than the conventional definition of a root mean square radius of a form factor.

The present limits on photon size and structure of the electron vertex come from the electron-proton scattering analysis,[3] which limits the "size" of any cutoff to distances $\lesssim 0.3$f. (i.e., the rms radius of any form factor $\lesssim 0.8$f.). Two experiments on wide angle pair production from hydrogen have been proposed[2,4] in order to extend our knowledge of the electron propagator to distances ~ 0.3f. The size of the μ-meson is limited by the measurement of its anomalous magnetic moment[2] to distances ~ 1.5f.

We here propose and discuss four feasible experiments which, when taken together with the earlier analyses on wide angle electron-positron pair production from hydrogen, will extend present knowledge of electron, photon, and μ-meson "size" to distances ~ 0.3f.

The new experiments under discussion here will extend our knowledge of all structures but the electron propagator. In the discussion of these proposed experiments we are limited by two factors:

(1) Large four-momentum transfers are required in order to probe electron, photon, and μ-meson size at small distances. This means small cross sections to which it must be ascertained there correspond finite and

---

[3] Yennie, Levy, and Ravenhall, Revs. Modern Phys. 29, No. 1, 144 (1957).
R. Hofstadter, Revs. Modern Phys. 28, 214 (1956).

[4] Bjorken, Drell, and Frautschi, Phys. Rev. 112, 1409 (1958). This reference is hereafter referred to as A.

not unreasonable counting rates. We limit our definition of "feasible" cross section to the lowest counting rate consistent with the experimental problems associated with the Stanford linear accelerator operating in the 500 Mev to 1 Bev energy range, as defined for us by B. Richter.[5]

(2) Heavy target particles must be used in order to achieve large energy in the center-of-mass system for the process. In order to avoid nuclear physics complications we confine our remarks to hydrogen targets. As in the previously proposed experiments, it is necessary that the proton structure be summarized unambiguously in terms of the form factors measured in elastic electron-proton scattering.[6]

The first of these experiments consists of electron-positron pair production by electrons in hydrogen (tridents). The two final electrons are observed at high energy and at angles $\frac{\pi}{2} \gg \theta \gg \frac{m}{E}$ relative to the incident beam. For actual experimental conditions $\theta \sim 10^\circ - 20^\circ$, being large enough to correspond to large four-momentum transfers and small enough to yield finite counting rates.

---

[5] We wish to thank Dr. B. Richter and also Professor W. K. H. Panofsky for informing us of experimental problems and limits of the Stanford linear accelerator.

[6] Conditions for which this is possible in electromagnetic pair production experiments have also been discussed by I. A. Dyatlov, JETP 35, 154 (1958) (in Russian). We wish to thank Dr. A. M. Bincer for calling this article to our attention.

In comparing this process with large angle e^+-e^- pair production by real photons one finds two points of primary interest here:

(a) The trident cross section for the above conditions of observation is dominated by Fig. 1a and Fig. 1b. Their magnitude is comparable with the cross section for e^+-e^- production by real photons and exceed the Weiszacker-Williams ratio of $\sim \frac{1}{137X}$. Here X is the number of radiation lengths in the converter for the photon process and is $\sim$0.1 for experimental conditions at the Stanford accelerator.[5] There are two reasons for the surprisingly large results obtained from Fig. 1a and Fig. 1b. First, additional retardation factors $1 - \beta\cos\theta$ arising from the virtual photons which connect with the incident electron help compensate the extra power of 1/137. Secondly, the "longitudinal" matrix element for producing a pair near the forward direction is considerably larger than the corresponding matrix element in the Bethe-Heitler process for real transverse photons. This follows from the fact that a sequence of vector interactions at high energy must produce an electron and positron of opposite helicities, which, in the forward direction, results in a singlet final state. By angular momentum conservation such a state does not couple well with a transverse photon, but will couple with the virtual longitudinal photons present in the trident process.

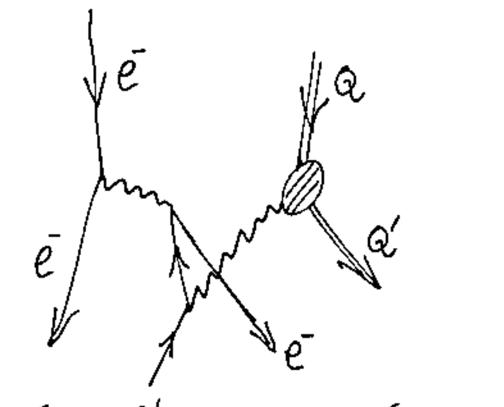

$|(p-p_1)^2| = 2p\cdot p_1 = 2EE_1(1-\cos\theta)$

(a)

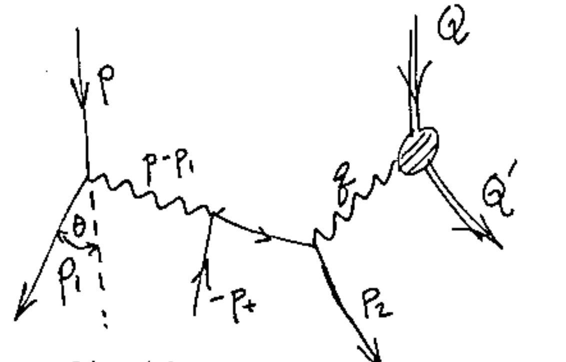

$|q^2| \simeq |(p-p_1-p_2)^2| \propto E^2(1-\cos\theta)^2$

(b)

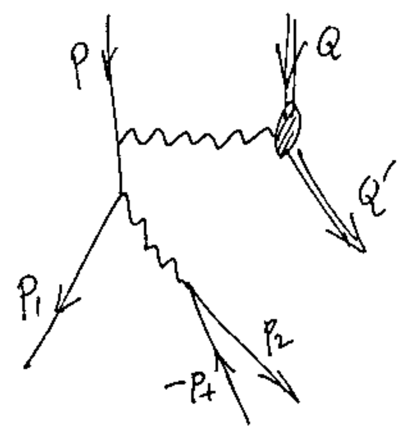

(c)

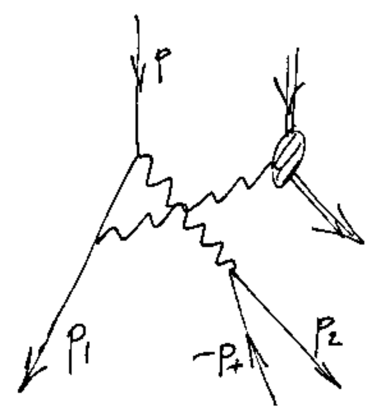

(d)

Figure 1: Feynman diagrams for trident production.

(b) As discussed previously, large angle pair production is a probe only of the electron propagator at small distances because the incident photon is real and corresponds to zero four-momentum. In contrast with this the photon from the initial electron in Fig. 1a and Fig. 1b is very virtual. Hence the ratio of electron to photon production of e^+-e^- pairs provides a sensitive test of photon propagator and electron vertex.

Aside from their intrinsic interest, the photon propagator and the electron vertex are of importance in connection with the understanding of the electron-proton scattering amplitude, which is presently interpreted by attributing all deviations from the Rosenbluth cross section for point protons to proton structure. Any structure of the photon propagator or electron vertex which is comparable with a size of 0.3f. will alter that interpretation and lead to the picture of a more compact nucleon structure.

The other three experiments are essentially repetitions of the two experiments of A and the experiment described above, with the electron-positron pair replaced by a μ-pair. They are possible because electrodynamic cross sections at high energies and large angles are roughly independent of mass; the dominant behavior is

$$\sigma = \frac{f(E_{incident}, \theta)}{(1-\beta\cos\theta)^n} \simeq \frac{f(E,\theta)}{\left(\frac{\theta^2}{2}+\frac{m^2}{2E^2}\right)^n}$$

Small distance effects are characteristically probed by a four-momentum transfer whose square is $q_\mu q^\mu = -E^2(1-\beta\cos\theta)$, where θ is a measured angle. Thus in comparing $\mu^+ - \mu^-$ and $e^+ - e^-$ production cross sections at high energies one has comparable counting rates and also probes structure at the same small distance by keeping energies and $(1 - \beta\cos\theta)$ constant. This means smaller angles at a fixed energy for the feasibility limit of μ-meson production in comparison with $e^+ - e^-$ production, according to the relation $1 - \beta_\mu \cos\theta_\mu = 1 - \cos\theta_e$.

In the present paper we do not carry out complete, detailed, quantitatively accurate calculations of the proposed cross sections as was presented for the $e^+ - e^-$ pair production in A. We wish here to present only approximate calculations in order to establish the feasibility of the experiments and in order to motivate them by analyzing what is learned from them. In Chapters II-V we describe the four new experiments. In Chapter VI all six experiments are summarized.

II. TRIDENT PRODUCTION

The appropriate Feynman diagrams for the e^+-e^- production by electrons are illustrated in Fig. 1. In addition to these there are four more obtained by exchanging the roles of electrons 1 and 2. In Fig. 2 are samples of other diagrams which will contribute small amounts to the cross section.

We choose a symmetrical arrangement with the incident electron and both final electrons in the same plane, and with the two final electrons emerging symmetrically to the right and left at an angle θ with the incident direction. This choice is motivated both by simplicity and by the desire to minimize transfer of momentum to the proton and hence its recoil current. With the twofold purpose of providing a large four-momentum $(p - p_1)^2$ to the virtual photon and of simplifying the calculations, we choose the electron and positron energies such that

$$m \ll E_+ \ll E_1 = E_2 \cong \frac{1}{2} E$$

The diagrams of Fig. 1a and Fig. 1b are "good" diagrams, since they are sensitive to the modifications of the photon propagator and electron vertex. If there is a form factor F associated with a photon line, the cross section will be modified by a factor

$$\sigma' = \sigma F((p-p_1)^2) \sim \sigma\,(1 + d^2 (p-p_1)^2)$$

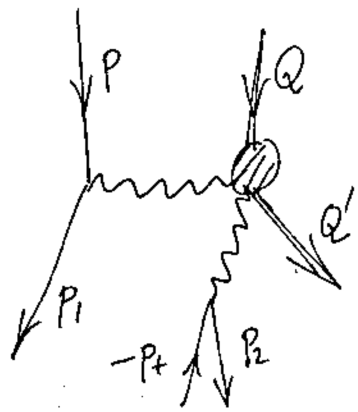

(a)

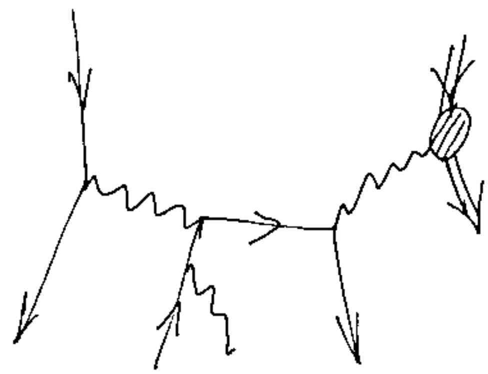

(b)

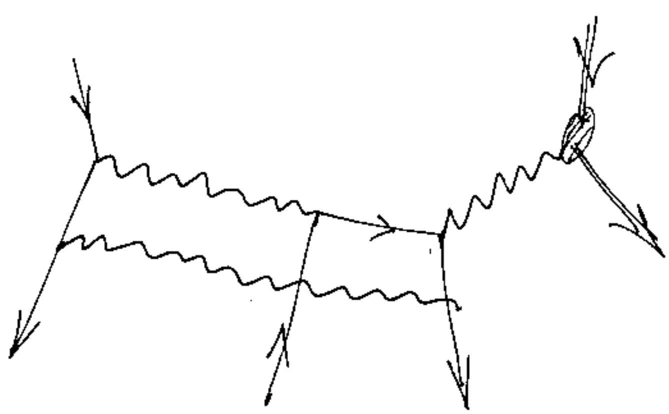

(c)

<u>Figure 2</u>: Correction graphs for trident production.

d is the reciprocal of the mass associated with the cutoff. If $d^2(p - p_1)^2 = -10\%$ we have, for $E_{inc} = 500$ Mev and $\theta = 20^\circ$,

$$d^2 = \frac{0.1}{2p\cdot p_1} \approx (0.5f.)^2 \quad .$$

For $E_{inc} = 1$ Bev and $\theta = 20^\circ$, $d^2 \propto (0.2f.)^2$.

The intermediate electron lines in the diagrams of Fig. 1 are also very virtual and may possibly contribute a form factor to the cross section. If a deviation from the value predicted by conventional electrodynamics is observed, one can attribute it either to a photon or an electron size; however, if the coincidence experiment of A confirms the quantum electrodynamic description of the electron propagator, this experiment will provide an unambiguous probe of the photon propagator and the electron vertex.

Fig. 1c and Fig. 1d are "bad" diagrams from the point of view of investigating the photon propagator and the electron vertex, since the positron can align itself with the final electron and make the intermediate photon connecting the electron lines nearly "real." These diagrams are thus very closely related to those of the large angle pair production experiments in A, and they probe the structure of the intermediate electron propagator. The intermediate photon connecting to the proton is virtual but, as was the case in A, its structure, along with that of the proton, is included in the empirical form factors for the proton vertex. However, for present purposes these "bad" diagrams are small in comparison with the "good" ones.

Because of the symmetrical arrangements the recoil momentum q^2 given the proton is very small ($|q| \sim 80$ Mev) and corrections due to proton form factors might be 5%. Such corrections may be included in an unambiguous way in the diagrams of Fig. 1 by the use of the measured proton form factors. Dynamical corrections due to the proton current, such as Fig. 2a, should be no more than a few percent. These terms are closely related to those for the proton Compton effect, and an estimate of their importance was made in the analysis of the coincidence experiment of A. Even including a factor of 10 for the pion resonance, the square of diagrams such as Fig. 2a amounted there to $\lesssim 1\%$. In the present experiment the contribution of such Compton terms to the counting rate is less than that of the pair experiment of A due to the extra power of e in the matrix element.[7] However, as discussed below, the total counting rate has not diminished. Thus even interference terms between these and the

---

[7]Because transverse photons are responsible for the Compton resonance, the longitudinal matrix elements are expected to have little effect on the Compton terms. See also R. Dalitz and D. R. Yennie, Phys. Rev. 105, 1598 (1957)

"good" diagrams of Fig. 1a and Fig. 1b will contribute less than 10%.

Radiative corrections should be fairly sizeable, since the effective energy resolution is the small positron energy. For E_+ = 15 Mev, one expects a Schwinger correction of the form

$$1 - \frac{4\alpha}{\pi} \ln\frac{E}{m} \ln\frac{E}{E_+} \simeq 0.85$$

Evidently a quantitative calculation of these effects is called for.

Using the standard techniques, we calculated the cross section assuming infinite proton mass and neglecting radiative corrections. The method of calculation is illustrated in Appendix II. Our result is:

$$\frac{d\sigma_\psi}{d\Omega_1 d\Omega_2 dE_1 dE_2} = \frac{\alpha^4}{2\pi^3 E^4 (1-x)^3} \Big\{ \ln\frac{2E_+}{m} \tag{1}$$

$$+ \frac{\epsilon^2}{(1+2\epsilon x)^4 (1-x)^2} \left[17 + 16x + 3x^2 - 24\epsilon - 2\delta\left(37 + 47x + \frac{22}{3}x^2\right)\right] \Big\}$$

In this expression E is the incident electron energy, $x = \cos\theta$, $\delta = \frac{E_+}{E}$, and $\epsilon(1-x) = \delta$. Only leading terms in ϵ and δ were retained. A typical set of feasible parameters within the scope of these approximations is E = 500 Mev, $\theta = 20^\circ$, E_+ = 15 Mev, $\epsilon = 0.5$, $\delta = 0.03$. The logarithm in (1) is the contribution of the square of the diagrams of Fig. 1c and Fig. 1d.

All non-logarithm terms were ignored. The interference of the "bad" exchange terms with the "bad" diagrams was also ignored, since the positron angular distributions compete and there can be no contribution with a large logarithm. Appendix I contains a proof of this statement. The rest of the terms in (1) correspond to

$$|M_{\text{"good"}}|^2 = |(1a) + (1b) + (1a)_{exch.} + (1b)_{exch}|^2$$

We find the happy circumstance that the "good" diagrams overpower the "bad" by a factor of 7. Interference terms between "good" and "bad" diagrams are somewhat more formidable and were not calculated; however, a rough upper limit can be placed on their contribution with the help of the theorem in Appendix I. The interference between "good" and "bad" diagrams can contain no large logarithmic factors. Thus, if $|M_{\text{"bad"}}|^2 \cong |A|^2 \ln \frac{E}{m}$ and $|M_{\text{"good"}}|^2 \cong B^2$ one must have $|M_{\text{interference}}|^2 \lesssim 2|AB|$, so that

$$\frac{|M_{\text{interference}}|^2}{|M_{\text{"good"}}|^2} \lesssim \frac{2|A|}{|B|} \lesssim 30\%$$

An easy way to ascertain the feasibility of this experiment is to compare the estimated trident counting rate (accurate to 50%) to that expected in the coincidence experiment of A for the same angles and incident energies. The result is:

$$\frac{R_\psi}{R_{BH}} = \frac{2\alpha}{\pi X}\;\frac{\epsilon^2(17+16x+3x^2)}{(1+x)(1-x)^2(1+2\epsilon x)^4} \tag{2}$$

X is the number of radiation lengths of radiator in the coincidence experiment of A. For an anticipated[5] $X \cong 0.1$, the ratio becomes ~ 5 for $\Theta = 20^\circ$ and thus exceeds the Richter limit of feasibility.[8]

---

[8]Dr. Richter has suggested an alternative and experimentally preferable arrangement to that discussed in this chapter in which one detects an electron and a positron in coincidence instead of two final electrons. We have verified that in this case too Fig. 1a and Fig. 1b are dominant and have calculated a feasible counting rate $\cong 30\%$ of the result of (2).

III. μ-PAIR PRODUCTION

An experiment in which a single μ-meson is detected at large angles and high energies probes the μ-meson vertex operator. The experimental arrangement is similar to that of the first experiment of A in which a positron is detected at 90° relative to the incident 140 Mev γ-ray beam. In the case of μ-mesons, there are two important differences. The first is that the large μ-meson mass forces one to higher energies and smaller angles in order to maintain a feasible counting rate. The second difference is that the "bad" diagram of the positron experiment becomes a "good" diagram in the μ-meson experiment (see Fig. 3a), since we are interested here in the process in which a μ scatters with large momentum transfer to the proton. In the electron case this is directly studied by the elastic electron-proton scattering experiments of Hofstadter et al.[4] and is known background in the study of the electron propagator. The experiment proposed here for μ-mesons serves as a substitute for elastic μ-meson-proton scattering which, for large momentum transfers, requires μ-meson beams of greater intensity than presently available.

Thus even an experiment of relatively poor accuracy will provide a sensitive test of the μ-meson vertex. For purposes of estimating a cross section, the Bethe-Heitler

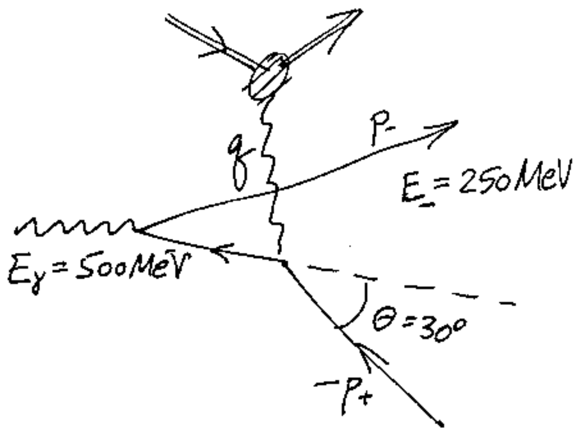

$$|q^2| = 2E_+^2(1-\cos\theta) \propto (1.4f.)^2$$

(a)

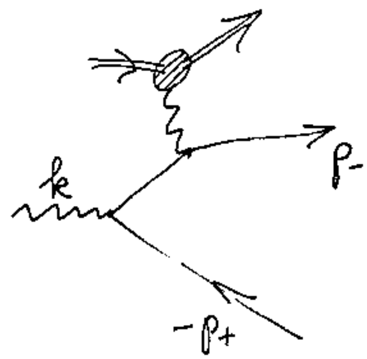

(b)

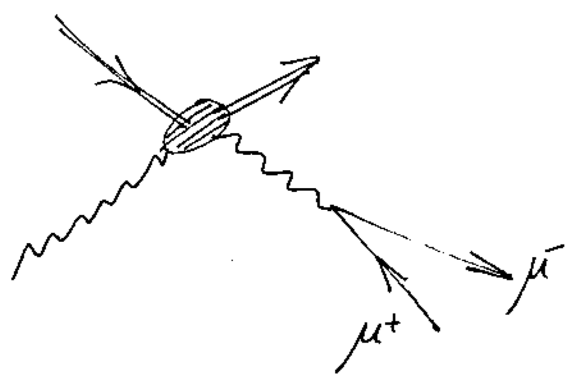

(c)

<u>Figure 3</u>: Feynman diagrams for μ-pair production.

formula, integrated over μ-angles for fixed μ^+ energy and angle, may be taken from the work of Hough.[9] For $E_\gamma = 500$ Mev, $\theta_+ = 30^\circ$, and $E_+ = E_- = 250$ Mev, one finds a counting rate of between 50% and 100% of that of the positron experiment of A. This estimate includes some corrections due to finite μ-meson mass; however, these are rather small.

The "size" investigated in this experiment is limited by the magnitude of the four-momentum q^2 transferred to the proton. For the predominant case of the μ^- emitted in the forward direction, $-q^2 = 2E_+^2 (1 - \beta_+ \cos\theta_+)$. For the above parameters, a 30% experiment probes μ-meson size to distances $\sim$1.1f.

Because the γ-ray energy is sufficiently high to make the π-meson resonance important, the effect of "Compton" terms illustrated in Fig. 3c may be as much as ten times greater than that encountered in the corresponding experiment of A with positrons. However, this still makes such correction terms no more than a 10-20% effect. Interference terms are diminished due to the effect discussed in Appendix I.

Our use of the Born approximation implies that the cross section for detection of μ^+ should equal that for μ^- under the same conditions of energy and angle.

---

9 P. V. C. Hough, Phys. Rev. 74, 80 (1948)

It would be interesting to check this experimentally, in order to test a breakdown of the Born approximation, perhaps due to a short range interaction of μ-mesons with the proton, or due to a breakdown of charge conjugation invariance at small distances. These remarks are also applicable to the electron production of μ-pairs described in Chapter V.

IV. PHOTOPRODUCTION OF μ-PAIRS IN COINCIDENCE

The μ-pair photoproduction coincidence experiment is completely analogous to the electron pair coincidence experiment described[10] in A. Because the experiment has been designed to keep the momentum transfer to the proton small, very little is learned of the μ-meson vertex; for that one needs the preceding experiment or electron production of μ-pairs (see Fig. 1). The cross section is nearly identical to that in A at sufficiently high energies, $\cong$ 1 Bev, since the Bethe-Heitler formula reduces to

$$\frac{d\sigma}{d\Omega_+ d\Omega_- dE_+} \propto \frac{\beta^2 \sin^2\theta}{(1-\beta\cos\theta)^4}$$

If θ_μ is chosen such that $1 - \beta_\mu \cos\theta_\mu = 1 - \cos\theta_e$, where θ_e is the corresponding angle in the electron pair experiment, the ratio of counting rates is nearly unity. For 1 Bev incident γ-rays and $\theta_e = 15^\circ$, θ_μ is 10°. The theoretical analysis is identical with that discussed in A, with the exception of small corrections $\sim\left(\frac{m_\mu}{E}\right)^2$ due to the larger μ-meson mass. What is probed

---

[10] This has been realized by several people, including Dr. S. C. Frautschi, who informed us of his own thoughts by letter from the Institute of Physics, Kyoto University, Japan, as well as the report (in Japanese) of Dr. Hiida. This is also remarked by Dyatlov in reference 5.

is the μ-meson propagator; the distance involved corresponds to a momentum $2k \cdot p_+ = k^2(1-\beta_\mu \cos\theta_\mu)$. Using the conventions in A, this corresponds to ~ 0.35f. for a 10% experiment at the above energy and angle.

V. μ-PAIR PRODUCTION BY ELECTRONS

The study of μ-pair production by electrons with an experimental arrangement similar to that for trident production probes the μ-meson vertex operator to smaller distances than the μ-pair photoproduction experiment described in Chapter III. Also, in principle, one learns the following new information in comparison with Chapter III. Here one probes the μ-meson vertex for a large momentum transfer carried by the virtual photon from the incident electron (see Fig. 1). The large momentum transfer to the μ-meson comes from the proton on the other hand in the large angle μ-production of Chapter III. An anomaly in the latter interaction may reflect a specific μ-proton interaction which is appreciable for large momentum transfers but which does not operate in a pure electron-μmeson-photon interaction. If the experiment is performed at ~ 1 Bev and $\theta_\mu = 9^\circ$, the cross section is about equal to that of the electron production experiment in Chapter II at the same energy and at an angle $\theta_e \cong 15^\circ$, which in turn is approximately a factor of eight larger than the expected Richter limit of a feasible counting rate in the coincidence experiment of A. The calculated expression for the cross section is modified somewhat from Chapter II in this case, since there are no exchange terms. We find, in the limit $\beta_\mu \longrightarrow 1$,

$$\frac{R}{R_{BH}} = \frac{\alpha}{\pi X(1+x)}\left\{ \ln\frac{2E_+}{m} + \frac{\epsilon^2}{(1-x)^2(1+2\epsilon x)^4}\left[9+8x+3x^2-\frac{40}{3}\epsilon-\frac{1}{3}\delta\left(56+106x+26x^2\right)\right]\right\}$$

The main difference from Chapter II is the loss of a factor of four due to the now missing exchange terms which were in phase with the direct terms in the trident production. For the parameters suggested above, one finds the "good" diagrams still contribute 2.5 times the "bad", with again the uncomputed interference terms being at most a 30% correction.

VI. CONCLUSION

Table I summarizes the results of this paper and of A. The column "modification" indicates in which way the calculated cross section is altered if there is a form factor F_γ in the photon propagator, F_{ep} in the electron propagator, F_{ev} in the electron vertex, and correspondingly for the μ-meson. The last column expresses the "size" probed for an experiment of the accuracy stated.

In all, six experiments have been proposed which, if all agree with theory, will have extended the limits of quantum electrodynamics, as applied to photons, electrons and μ-mesons to distances $\sim$ 0.3f. Any disagreement between theory and experiment can be attributed only to a failure in the present theory of quantum electrodynamics of the photon and electron, or, in the last three experiments, to hitherto unknown interactions of the μ-meson.[11]

[11] K. Hiida (to be published) has suggested radiative K-μ decay as another possible experiment for study of μ-meson structure.

TABLE I: SUMMARY OF PROPOSED EXPERIMENTS

Type of Experiment	Modification	Accuracy	Sensitivity
$\gamma+p\rightarrow e^{+}+e^{-}+p$ E_{γ} = 140 Mev 70 Mev e^{+} at 90°	$0.8+0.2F^{2}_{ep}$	5%	~0.7f.
$\gamma+p\rightarrow e^{+}+e^{-}+p$ E_{γ} = 500 Mev 245 Mev $e^{+}-e^{-}$ at 20°	F^{2}_{ep}	10%	~0.5f.
$\gamma+p\rightarrow e^{+}+e^{-}+p$ E_{γ} = 1 Bev 500 Mev $e^{+}-e^{-}$ at 15°	F^{2}_{ep}	10%	~0.3f.
$\gamma+p\rightarrow \mu^{+}+\mu^{-}+p$ E_{γ} = 500 Mev 250 Mev μ^{+} or μ^{-} at 30°	$F^{2}_{\mu v}/F^{2}_{ev}$	30%	~1.1f.
$e^{-}+p\rightarrow e^{+}+e^{-}+e^{-}+p$ E_{inc}= 500 Mev 240 Mev $e^{-}-e^{-}$ each at 20°	$F^{2}_{ep}\ F^{4}_{ev}\ F^{2}_{\gamma}$	10%	~0.5f.
$e^{-}+p\rightarrow e^{+}+e^{-}+e^{-}+p$ E_{inc}= 1 Bev 490 Mev $e^{-}-e^{-}$ each at 15°	$F^{2}_{ep}\ F^{4}_{ev}\ F^{2}_{\gamma}$	10%	~0.2f.
$\gamma+p\rightarrow \mu^{+}+\mu^{-}+p$ E_{γ} = 1 Bev 500 Mev $\mu^{+}-\mu^{-}$ at 10°	$F^{2}_{\mu p}$	10%	~0.3f.
$e^{-}+p\rightarrow e^{-}+\mu^{+}+\mu^{-}+p$ E_{inc}= 1 Bev 450 Mev $\mu^{+}-e^{-}$ or $\mu^{-}-e^{-}$ at 9°	$F^{2}_{\mu p}\ F^{4}_{\mu v}\ F^{2}_{\gamma}$	10%	~0.3f.

APPENDIX I: THE ABSENCE OF LOGARITHMS IN INTERFERENCE TERMS

Consider any general graph such as illustrated in Fig. 4, in which the electron and positron are extreme relativistic, and for which the positron angles are to be integrated over. In Fig. 4a there will be a strong singularity when $\vec{p}_+$ is parallel to $\vec{p}_-$, since the intermediate photon is then nearly real. If

$$M_{4a} = \frac{M_\mu \langle p_+ | \gamma^\mu | p_- \rangle}{(p_+ + p_-)^2}$$

then

$$\mathrm{Tr} \int d\Omega_+ |M_{4a}|^2 \cong \int d\Omega_+ M_\mu M_\nu \frac{\mathrm{Tr}\, \not{p}_+ \gamma^\mu \not{p}_- \gamma^\nu}{(2p_+ \cdot p_-)^2} + \int \frac{O(m^2)\, d\Omega_+}{(2p_+ \cdot p_-)^2}$$

If $\vec{p}_+$ is parallel to $\vec{p}_-$ we also have $(p_+ + p_-) \cdot M = o(m^2)$ by gauge invariance. Hence if $p_+ \cdot p_- \cong \frac{1}{2} E_+ E_- \theta^2$, we have $p_+ \cdot M = o(\theta) + o(m^2)$. Thus

$$\mathrm{Tr} \int d\Omega_+ |M_{4a}|^2 \cong \int d\Omega_+ \left[\frac{8 p_+ \cdot M\, p_- \cdot M}{(2p_+ \cdot p_-)^2} - \frac{M_\mu M^\mu}{p_+ \cdot p_-} + \frac{O(m^2)}{(p_+ \cdot p_-)^2} \right]$$

$$\cong \int 2\pi \theta\, d\theta \left[\frac{O(\theta^2)}{O(\theta^4)} + \frac{1}{O(\theta^2)} + \frac{O(m^2)}{O(m^2)} \right.$$

$$\sim \int_{\frac{m}{E}} \frac{d\theta}{\theta}$$

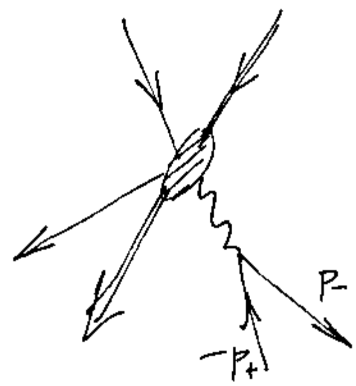

(a)

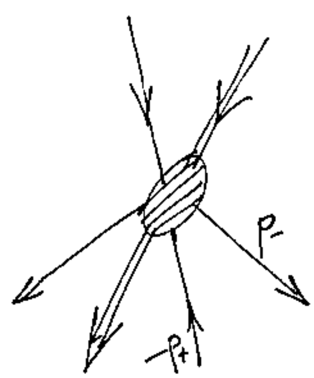

(b)

Figure 4: General pair production diagrams.

Thus M_{4a}^2 exhibits at most a logarithmic singularity. M_{4a}^2 corresponds to the square of the two "bad" diagrams in, say, the trident experiment.

Now consider an interference term between M_{4a} and M_{4b}, where M_{4b} is any single graph which exhibits no singularity as $\vec{p}_+$ becomes parallel to $\vec{p}_-$. The interference term becomes

$$M_{int}^2 = \mathrm{Tr} \int \frac{d\Omega_+}{p_+ \cdot p_-} \left\{ \left[\not{p}_+ \gamma^\mu \not{p}_- M_{4b} M_\mu \right] + O(m^2) \right\}$$

There exists no logarithmic singularity in M_{int}^2 . Since we have only a logarithmic singularity in the denominator to begin with, we may immediately put $\vec{p}_+$ parallel to $\vec{p}_-$ in the numerator, since any corrections are $o(\theta)$. Then

$$\mathrm{Tr} \left[\not{p}_+ \gamma^\mu \not{p}_- M_{4b} M_\mu \right] = 2 M_\mu p_+^\mu \, \mathrm{Tr} \not{p}_- M_{4b} = O(\theta)$$

since again $p_+^\mu M_\mu = o(\theta)$ by gauge invariance.

Thus only those amplitudes in the "bad" diagram which do not contribute to the logarithmic singularity will contribute to the interference terms; hence, one may conclude that interference terms involving bad diagrams must be relatively small.

APPENDIX II: CALCULATION OF PAIR PRODUCTION BY ELECTRONS

The pair production calculation was set up in the customary way. An integration over positron angles is required, and it was found to be convenient to carry this out before trying to do the traces, using the fact

$$\mathrm{Tr}\ \not{p}_+ O = \sum_u p_+ \cdot u \ \mathrm{Tr}\ \not{u} O$$

where the summation is over a complete orthonormal set of basis vectors. The worst of the integrals encountered is

$$I = \int \frac{d\Omega_+ \ p_+ \cdot p}{q^4 (q+p_1)^2 (q+p_2)^2} = 6 \int_0^1 dy \int_0^1 dz \, z(1-z) \int \frac{d\Omega_+ \ p_+ \cdot p}{\left[q^2 + 2q \cdot (p_1 y + p_2 (1-y)) z \right]^4}$$

See Fig. 1 for the notation. The angle integration is elementary and one is left, after throwing out correction terms $o(E_+^2)$, with a sum of terms, a typical one being

$$J = \int_0^1 \int_0^1 \frac{z(1-z) \, dy \, dz}{\left[k^2 + 2k \cdot (p_1 y + p_2 (1-y)) z - 2E_1 E_+ z \right]^4}$$

where $k = p - p_1 - p_2$.

Because $k \cdot p_1 = k \cdot p_2$, the y integral is trivial. Then letting $\alpha = k^2$ and $\beta = k^2 + 2k \cdot p_1 - 2E_1 E_+$, the Feynman parameterization may be "undone." One obtains

$$J = \int_0^1 \frac{dz\; z(1-z)}{[\alpha(1-z) + \beta z]^4} = \frac{1}{6\alpha^2 \beta^2}$$

In this way all integrals are easily done and one gets

$$I = \frac{E_+}{\alpha^2 \beta^2} \left\{ E + \frac{4}{3} \frac{E_\pm}{\beta} (EE_1 - p \cdot p_1) - \frac{4}{3} E_+ \, p \cdot k \, \frac{\alpha + \beta}{\alpha \beta} + O(E_+^2) \right\}$$

SPECTRAL REPRESENTATIONS OF GREEN'S FUNCTIONS IN PERTURBATION THEORY*

I. INTRODUCTION

There has recently been a great deal of interest in the analytic properties of the Green's functions and scattering amplitudes of quantum field theory.[12] The program of such studies, roughly speaking, is to analytically continue physics into the complex plane and study its properties there. Mathematically this is a very powerful method; however, from the standpoint of physics it has the disadvantage that our physical intuition is not so easily analytically continued.

We here present an approach to the subject based upon the Feynman diagram expansion which has a certain amount of intuitive appeal in the "unphysical regions". The approach also exhibits the role of causality in determining analytic properties of scattering amplitudes, as well as showing the role of "real intermediate states" in determining their singularities. Much of the work is a

*Submitted for publication in Annals of Physics.

[12] For other references see Proceedings of the 1958 Annual Conference on High Energy Physics at CERN (Geneva, 1958). Also see Oehme and Taylor, Phys. Rev. 113, 371 (1959).

paraphrase of that of Chisholm and Nambu,[13] who investigated the properties of Green's functions in the perturbation expansion.[14]

In Chapter II we shall attempt to outline the physical idea involved in the development at the expense of mathematical precision. In Chapter III we shall carry out the integration of a Feynman graph over four-momenta of internal loops in a general way. In Chapter IV we derive the Nambu representation[13] which exhibits the analytic properties of the general Feynman diagram. In Chapter V we show that the analytic properties are completely determined by the existence of real causal intermediate states. In Chapter VI we discuss the vertex operator as function of momentum transfer and determine its analytic properties to all finite orders of the coupling constant. In Chapter VII we discuss scattering of particles of equal mass.

---

[13] R. Chisholm, Proc. Cambridge Soc. 48, 300 (1952)
Y. Nambu, Nuovo Cimento 6, 1064 (1957)
Y. Nambu, Nuovo Cimento 9, 610 (1958)

[14] Karplus, Sommerfield, and Wichmann (Phys. Rev. 111, 1187 (1958) and Phys. Rev. (to be published)) have investigated in detail the lowest order graphs for the vertex function and scattering amplitude.

II. THE PHYSICAL SIGNIFICANCE OF THE METHOD

In general, a scattering amplitude or Green's function, which we shall denote by $\mathcal{M}$, may be written in momentum space as a finite sum of covariants composed of products of spin matrices and momentum vectors, each multiplied by a form factor which is a function of all the scalar invariants at our disposal. For example the electromagnetic vertex operator for a proton may be written as

$$\Gamma_\mu(q^2) = \gamma_\mu F_1(q^2) + \frac{i}{4m}\sigma_{\mu\nu} q^\nu F_2(q^2) \qquad (1)$$

The square of the four-momentum of the photon is the only independent scalar invariant in this case.

What we shall hereafter mean by the investigation of the analytic properties of such amplitudes is the investigation of the properties of the invariant form factors associated with these amplitudes. In particular the question to which we shall address ourselves is what the analytic properties of these form factors are when the value of one of the invariants is extended into the complex plane, all other invariants remaining fixed and real. We shall answer this question to all finite orders of perturbation theory. Of course, this does not prove anything about the complete amplitude, but may provide a useful guide.

The approach we shall follow is based upon the Feynman diagram expansion, which is very closely related to the Lagrangian form of quantum mechanics. Very crudely stated, one writes a scattering amplitude as a sum over all classical paths of the probability amplitude for the path.[15] This probability amplitude is proportional to e^{iJ}, where J is the value of the action function of the system. The difficulty of this approach to quantum mechanics is that there are many paths to sum, and to do this in a precise mathematical way is not easy. In the n^{th} order contribution to a perturbation expansion, these paths are expressed as free-particle paths which are connected together by n local interactions which destroy and create the particles. A free particle path may be expressed in the following way:

$$x_2^{\mu} - x_1^{\mu} = p^{\mu} z \qquad (2)$$

This simply states that the four-momentum p_{μ} is proportional to the coordinate displacement Δx_{μ} of the particle.

---

[15] R. P. Feynman, Revs. Modern Phys. 20, 267 (1948)

The parameter z must be positive in order to guarantee causality: positive energies propagate forward in time and negative energies backward. The causality statement, i. e. the positive character of z, will be extremely important in the development that follows. Equation 2 has an analogue in the domain of electrical circuit theory which will also prove immensely useful, namely Ohm's law:[16]

$$V_2 - V_1 = ir \qquad (2a)$$

Coordinate plays the role of voltage, momentum that of current, and the positive parameter z that of resistance. From this point of view a Feynman diagram looks very much like an electrical circuit, if in each line of the diagram we assign a parameter z to describe the path. Kirchoff's laws are transcribed into the statements that at each vertex of the diagram momentum is conserved and that the sum of coordinate displacements around any closed loop is zero. For a given Feynman graph, the description of the paths of the particles is completely specified if the momentum q_i of each external particle is specified and the "resistance" z of each internal line, or branch, is given. It is then not surprising, from the point of view of Lagrangian quantum mechanics, that

---

[16] J. Mathews, Phys. Rev. 113, 381 (1959)

the contribution of a Feynman diagram may be written as a sum over all resistances of e^{iJ}, where J is the action function for the "circuit" problem. That is, it is possible to write

$$\mathcal{M} = \int_0^\infty dz_1 \cdots dz_n \, e^{iJ(z_1 \cdots z_n, q_i)} \mathcal{N}(q_i, z_i) \qquad (3)$$

J, the action function for the corresponding electrical circuit problem, is well-known[17] (by electrical engineers, perhaps) to be

$$J = \frac{1}{2} \sum_{i=1}^{n} \left[k_i^2 z_i - m_i^2 z_i \right] \qquad (3a)$$

k_i is the current in the i^{th} branch, and satisfies Kirchoff's laws. m_i is the mass associated with the particle in the i^{th} branch. The first term corresponds to the sum of i^2r power losses in all the lines; the second term is a constant added by the physicist to make a "real" particle carry no action. N corresponds to miscellaneous polynomials and spin matrices associated with the specific form of the interaction. It is discussed in detail in Appendix II.

[17] E. A. Guillemin, Introductory Circuit Theory (Wiley, New York, 1953).

In order to derive circuit equations from J, one varies with respect to the k_i, subject to the constraints of momentum conservation at vertices. These may be introduced with the aid of Lagrange multipliers so that

$$J = \frac{1}{2}\sum_i (k_i^2 - m_i^2) z_i - \sum_{i,j} x_j \cdot \epsilon_{ij} k_i - \sum_{i,j} x_j \cdot \tilde{\epsilon}_{ij} q_i \qquad (4)$$

The summation runs over vertices j, the x_j are Lagrange multipliers (physically, the value of the coordinate (voltage) at the vertex), and

$$\epsilon_{ij} \begin{cases} +1 \text{ if current } k_i \text{ flows into } j^{th} \text{ vertex} \\ -1 \text{ if current } k_i \text{ flows out of } j^{th} \text{ vertex} \\ \;\;0 \text{ if } i^{th} \text{ branch is not connected to } j^{th} \text{ vertex} \end{cases} \qquad (5)$$

A similar definition holds for $\tilde{\epsilon}_{ij}$, with k_i replaced by q_i. Variation of J with respect to the k_i yields

$$k_i z_i = \sum_j{}' \epsilon_{ij} x_j = x_{final} - x_{initial} \qquad (6)$$

$$\sum_i{}' (\epsilon_{ij} k_i + \tilde{\epsilon}_{ij} q_i) = 0$$

which, indeed, is "Ohm's law" for the i^{th} branch.

Equation 3 is the basic expression for investigation of the analytic properties. We shall derive it more convincingly in the next chapter. However, before going on, we wish to say that the circuit analogy is quite powerful; all the "intuitively obvious" theorems from electrical circuit theory[17] are available to us. For instance, in the case of the vertex operator we may use the fact that any black box with three terminals and only resistors inside may be reduced to an equivalent circuit as shown in Fig. 5. (ζ_1, ζ_2, ζ_3) are the "equivalent

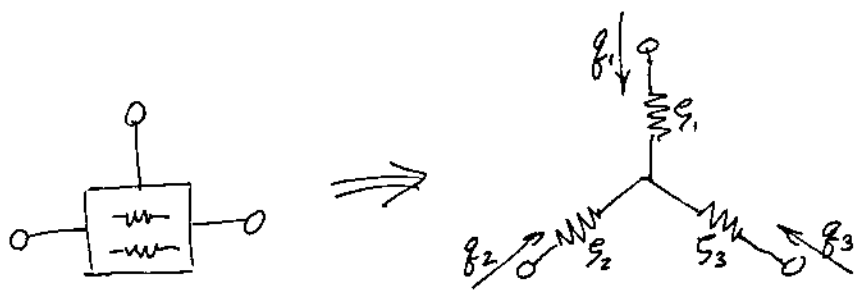

Figure 5: Lumped circuit for the vertex function.

resistances", and they are positive functions (f_1, f_2, f_3) of the z_i of the original network. Hence

$$\mathcal{M} = \int_0^\infty d\zeta_1\, d\zeta_2\, d\zeta_3\, dM^2\, e^{\frac{i}{2}\left(\sum_i q_i^2 \zeta_i - M^2\right)} \rho(\zeta_1, \zeta_2, \zeta_3) \qquad (7)$$

where

$$\rho = \int_0^\infty dz_1 \cdots dz_n\, \delta\left(M^2 - \sum_i m_i^2 z_i\right) \prod_{i=1}^{3} \delta\left(\zeta_i - f_i(z)\right) N(q_i, z_i) \qquad (8)$$

and we are well on our way to a spectral representation for the amplitude $\mathcal{M}$.

III. INTEGRATION OF THE FEYNMAN DIAGRAM

We begin our systematic investigation by writing down the expression for a given Feynman graph in momentum space.

$$\mathcal{M} = \int \frac{d^4p_1 \cdots d^4p_n}{\prod_i (p_i^2 - m_i^2)} \prod_j \delta^{(4)}\Big(\sum_i \epsilon_{ij} p_i + \sum_k \tilde{\epsilon}_{kj} q_k\Big) M(p_i, q_i) \tag{9}$$

ϵ_{ij} is defined by (5). p_i represents the current in the i^{th} internal branch of the diagram and q_k the source current of one of the external branches, defined as positive if the current flows into the graph. Hence $\sum_k q_k = 0$. $M(p_i, q_i)$ contains all other factors, such as intermediate state projection operators, spin matrices, and coupling constants. What resides in M will not affect analytic properties except to determine the behavior at ∞.

We carry out the momentum-space integrals by introducing the following representation for the propagator:

$$\frac{1}{p_i^2 - m_i^2 + i\varepsilon} = \frac{-i}{2} \int_0^\infty dz_i \, e^{\frac{i}{2}(p_i^2 - m_i^2) z_i} \tag{10}$$

From the discussion in Chapter II, we are led to associate these parameters z_i with the "resistances". Introducing the usual representation for δ-function we have

$$\mathcal{M} = \left(\frac{-i}{2}\right)^n \int_0^\infty dz_1 \cdots dz_n \int_{-\infty}^{\infty} d^4p_1 \cdots d^4p_n \frac{d^4y_1 \cdots d^4y_j}{(2\pi)^{4j}} \exp i\Big\{\frac{1}{2}\sum_i (p_i^2 - m_i^2) z_i - \sum_{ijk} y_j (\epsilon_{ij} p_i + \tilde{\epsilon}_{kj} q_k)\Big\} M(p_i, q_i) \tag{11}$$

After the propaganda buildup of Chapter II, we expect the "Kirchoff-law" momenta defined by (5) to be of basic importance. We thus change variables in p-space by letting

$$p_i = k_i + l_i \tag{12}$$

This change corresponds to that of "completing the square" in the conventional method of integration. The k_i depend only upon external momenta q_i and the resistances z_i. Then, with the aid of Kirchoff's laws (6), the argument of the exponential is

$$\begin{aligned} &\frac{1}{2}\sum_i (p_i^2 - m_i^2) z_i - \sum_{ijk} y_j (\epsilon_{ij} p_i + \tilde{\epsilon}_{kj} q_k) \\ &= \frac{1}{2}\sum_i (k_i^2 - m_i^2) z_i + \sum_{ij} l_i \cdot \epsilon_{ij} (x_j - y_j) + \frac{1}{2}\sum_i l_i^2 z_i \end{aligned} \tag{13}$$

After doing the integrations over the y's we obtain

$$\mathcal{M} = \int_0^\infty dz_1 \cdots dz_n \; e^{\frac{i}{2}\sum_i (k_i^2 - m_i^2) z_i} \, N(q_i, z_i) \tag{14}$$

where

$$N(q_i, z_i) = \left(\frac{-i}{2}\right)^n \int d^4 l_1 \cdots d^4 l_n \prod_j \delta^{(4)}\left(\sum_i \epsilon_{ij} l_i\right) e^{\frac{i}{2}\sum_i l_i^2 z_i} M(k_i + l_i, q_i)$$

(15)

N is a polynomial in the k_i, l_i, and q_i; hence $N(q_i, z_i)$ will be a polynomial in the q_i. We may, in the way indicated in Chapter II, then write N as a finite sum of covariants involving spin matrices multiplied by invariant form factors. These form factors will be finite polynomials in the scalars formed from the q_i. The coefficients of the terms in the polynomials are functions of the z_i. An explicit prescription for writing down N after integration of the internal momenta is given in Appendix II.

IV. THE NAMBU REPRESENTATION

Having obtained $\mathcal{M}$ as an integral over the resistance parameters, we are ready to study its analytic properties. We shall find that the factor $J = \frac{1}{2}\sum_i (k_i^2 - m_i^2) z_i$ completely determines the analytic properties of $\mathcal{M}$. This is best seen by transforming (14) to the perhaps more familiar expression obtained by Feynman's methods of integration. We use a property called "scaling invariance" by Nambu.[13] One writes

$$1 = \int_0^\infty \frac{d\lambda}{\lambda} \Phi\left(\frac{z_i}{\lambda}\right) \tag{16}$$

where Φ is any positive function which satisfies this condition for all positive z_i. For instance

$$\Phi = \delta\left(1 - \sum_i \frac{z_i}{\lambda}\right) \tag{17}$$

is such a function. Then from (14),

$$\mathcal{M} = \int_0^\infty \frac{d\lambda}{\lambda} dz_1 \cdots dz_n \, \Phi\left(\frac{z_i}{\lambda}\right) e^{iJ} N(g_i, z_i) \tag{18}$$

We now let $z_i \to \lambda z_i$. Under a uniform scale change of resistances, the internal currents k_i do not change because the external current sources remain constant; therefore $J \to \lambda J$. Also (see Appendix II)

$$N \to \frac{a_\alpha}{\lambda^\alpha} + \cdots + \frac{a_\beta}{\lambda^\beta} \tag{19}$$

One may then carry out the λ-integration, provided $\alpha < n$, and the result will be:

$$\mathcal{M} = \int_0^\infty dz_1 \cdots dz_n \; \Phi(z_i) \left\{ \frac{b_\alpha}{J^{n-\alpha}} + \cdots + \frac{b_\beta}{J^{n-\beta}} \right\} \tag{20}$$

which exhibits the fact that singularities exist only if J can vanish within the integration region. Terms for which $\alpha \geq n$ correspond to the infamous ultraviolet divergence and are eliminated by the renormalization procedure. This will not affect our result that singularities are determined by the behavior of J.

An important representation for $\mathcal{M}$ may now be obtained by borrowing the lumped circuit notion from network theory. The first term in J, namely $J_0 = \frac{1}{2}\sum_i k_i^2 z_i$ is just the power burned up in the circuit. It is a quadratic form in the external currents q_i and has special properties which may be found by considering the electrical circuit model, where the q_i are one-dimensional real currents. In this case we know that $J_0 > 0$, since the power burned up in an electrical circuit cannot be negative. J_0 is expressible in a way which explicitly exhibits this fact; in particular

$$J_0 = \sum_\alpha \xi_\alpha Q_\alpha^2 \tag{21}$$

where $\zeta_\alpha > 0$, and Q_α is a sum of some subset of the external q_i entering the graph. That is

$$Q_\alpha = \begin{cases} q_i & \text{or} \\ q_i + q_j & \text{or} \\ q_i + q_j + q_k, & \text{etc.} \qquad (i \neq j \neq k) \end{cases} \tag{21a}$$

The sum in (21) runs over possibly <u>all</u> such invariants Q_α^2. This result is derived as Theorem I in Appendix III. In general, not all these Q_α^2 are linearly independent, and identities relating them to each other may be used to reduce J_0.

In the case of the three-terminal network, there are only three Q_α^2, all independent. The ζ_α are readily interpreted as "equivalent resistances" in a lumped circuit. This situation is illustrated in Fig. 5. In the case of the four-terminal network (scattering amplitude), there are seven Q_α^2 (the four masses m_i^2, the energy σ^2, the crossed energy $\bar{\sigma}^2$, and the momentum transfer Δ^2), and there is one constraint between them, namely $\sum_i m_i^2 = \sigma^2 + \bar{\sigma}^2 + \Delta^2$. Depending upon the magnitudes of the ζ_α, one eliminates either σ^2, $\bar{\sigma}^2$, or Δ^2, and the resultant expression for J_0 may be interpreted as the power burned up in a lumped circuit with positive resistances, the three cases illustrated in Fig. 6.

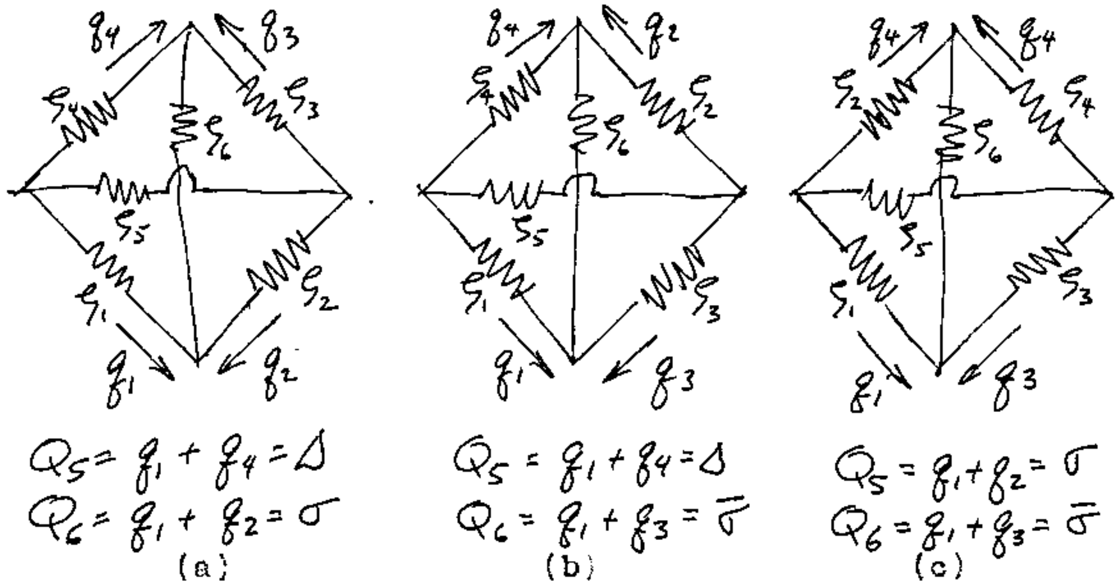

<u>Figure 6</u>: Lumped circuits for the scattering amplitude.

When there are more than four external lines the reduction to lumped circuits is more involved. We shall not discuss such cases in detail.

By making a change of variables from the z_i to the ζ_α and introducing $M^2 = \sum_i m_i^2 z_i$, one has the following representation for the vertex:

$$\mathcal{M} = \sum_m \int_0^\infty \frac{d\zeta_1\, d\zeta_2\, d\zeta_3\, dM^2\, \rho_m(\zeta_\alpha, M^2, Q_\alpha^2)}{\left[\sum_{\alpha=1}^{3} \zeta_\alpha Q_\alpha^2 - M^2 + i\epsilon\right]^m} \tag{22}$$

For the scattering amplitude, the representation may be written as $\mathcal{M} = \sum_{k=1}^{3} \mathcal{M}_n$, where each $\mathcal{M}_n$ has the form:

$$\mathcal{M}_n = \sum_m \int_0^\infty \frac{d\zeta_1 \cdots d\zeta_6\, dM^2\, \rho_m(\zeta_\alpha, M^2, Q_\alpha^2)}{\left[\sum_{\alpha=1}^{4} \zeta_\alpha m_\alpha^2 + Q_5^2 \zeta_5 + Q_6^2 \zeta_6 - M^2 + i\epsilon\right]^m} \tag{23}$$

Each $\mathcal{M}_n$ corresponds to one of the cases illustrated in Fig. 6.

For the general scattering amplitude one has the representation[13]

$$\mathcal{M}(q_1 \cdots q_n) = \sum_m \int_0^\infty \frac{d\xi_1 \cdots d\xi_{2^n-1}\; dM^2\, \rho_m(\xi_\alpha, M^2; q_i)}{\left[\sum_{\alpha=1}^{2^n-1} \xi_\alpha Q_\alpha^2 - M^2 + i\varepsilon\right]^m} \tag{24}$$

V. LOCATION OF THE SINGULARITIES

Having obtained the Nambu representation for $\mathcal{M}$, we now ask what analytic properties may be inferred from it. Considered as a function of one of the Q_α^2, $\mathcal{M}_n$ will be analytic in the upper half plane because of the positive character of the resistance coefficient multiplying Q_α^2 and the $i\epsilon$ in the denominator. If for some real value of Q_α^2 it happens that $\mathcal{M}_n = \mathcal{M}_n^*$, i.e. the $i\epsilon$ may be dropped from J, then $\mathcal{M}_n$ may be continued into the lower half plane as well, and all singularities of $\mathcal{M}_n$ will consist of branch points within a distance $o(\epsilon)$ of the real axis. It is in such cases that the subsequent discussion will be especially useful, since the methods to be described apply most easily to singularities $o(\epsilon)$ of the real axis. If no such Q_α^2 exists, it is not possible to state that all singularities are confined to the real axis.

What we now prove about the analytic properties of $\mathcal{M}$ is that all singularities $o(\epsilon)$ of the real axis of any of the Q_α^2 are due to the existence of real causal intermediate states. An easily applied prescription for determining the existence of such states will be given. We again emphasize that if $\mathcal{M}_n(Q_\alpha^2) = \mathcal{M}_n^*(Q_\alpha^2)$ for some real Q_α^2, then the procedure to be outlined will yield a necessary condition on all singularities of $\mathcal{M}_n$ as function of one of the Q_α^2. We first consider this case and choose Q_α^2 such that J is either positive or negative definite, and $M = M^*$. It is easy to see that, indeed, J is negative definite, since we may compute its value at the point $(z_1, 0, 0, \cdots 0)$ in z-space. All branches in the circuit become "short circuited" except the first and the circuit (if the graph is proper) collapses to that illustrated in Fig. 7. Obviously no current will go through the

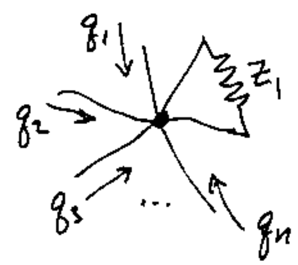

Figure 7: Illustration that J is negative definite

resistor z_1 and no power is dissipated. Hence $J = -m_1^2 z_1 < 0$. The case of photons is an exception, but formally may be handled by giving the photon a small mass.

In order to find the first branch point, we slowly change the external q_1 and watch the behavior of J in z-space. After we search a while we may reach some value of the external q_1 such that $J(z_i)$ no longer is negative definite, but attains zero at some point $(z_1^0, \cdots z_n^0)$

in z-space. In general, this point may lie on a boundary of integration; i. e. some of the z_i^o may be zero. However, for those z_i^o which are not zero (and there must be at least one) J will attain a maximum; that is, $\frac{\partial J}{\partial z_i^o} = 0$. Thus we may write

$$\delta J = \delta \left[\frac{1}{2} \sum_i (k_i^2 - m_i^2) z_i^o \right] = 0 \tag{25}$$

where what is meant by δJ is the change in J due to variations in those z_i^o which are not equal to zero. We must remember that the k_i, as solutions of Kirchoff's laws, depend upon the z_i; however, the fact that J is the action function for the circuit problem is of great help. If we first write in the Lagrange multiplier terms and then vary J, we obtain with the aid of (6)

$$\begin{aligned} \delta J &= \frac{1}{2} \sum_i (k_i^2 - m_i^2) \delta z_i^o + \sum_i k_i z_i^o \delta k_i \\ &= \frac{1}{2} \sum_i (k_i^2 - m_i^2) \delta z_i^o + \sum_j x_j \delta \left(\sum_i \epsilon_{ij} k_i + \sum_k \tilde{\epsilon}_{kj} q_k \right) \\ &= \frac{1}{2} \sum_i (k_i^2 - m_i^2) \delta z_i^o \end{aligned} \tag{26}$$

Thus $k_i^2 = m_i^2$ for those z_i which are in the interior of the integration region and $z_i = 0$ for those which are on the boundary.[18] We see that a necessary condition for a singularity in $\mathcal{M}$ is that the graph be decomposable into short circuited "blobs" (within which all $z_i = 0$) connected by "real" lines for which $k_i^2 = m_i^2$ and such that Kirchoff's laws, i.e. the correct causal behavior, are maintained throughout. This result may be generalized to the following theorem, proved in Appendix III:[19]

<u>Theorem 2</u>: For $\epsilon > 0$, $\mathcal{M}(Q_1^2 \cdots Q_\alpha^2)$ is an analytic function of all its arguments in a neighborhood of any real point $(Q_1^2, \cdots Q_\alpha^2)$. A necessary condition for a singularity which is $o(\epsilon)$ of such a real point is the existence of a real intermediate state which satisfies Kirchoff's laws with real positive "resistors" z_i.

In order to make the result useful we must find criteria for determining the possible existence of real intermediate states. The simplest example is that of the propagator or, equivalently, the mass operator, for which there exists a rigorous proof of the analytic properties.[20]

---

[18] The boundary $\sum z_i = 1$ is irrelevant since $\sum_i \frac{\partial J}{\partial z_i} = 0$ if $J = 0$ because of scaling invariance.

[19] I am indebted to Dr. S. Mandelstam for suggesting this theorem.

[20] H. Lehmann, <u>Nuovo Cimento</u> <u>11</u>, 342 (1954)

A mass operator M is a function of a single variable q^2, the four-momentum of the particle. We know for $q^2 < 0$ that $M(q^2)$ is analytic, since J is automatically negative definite. Singularities in M must therefore be confined to the positive real q^2 axis. For $q^2 \geq 0$, one may choose $q = (q_o, 0, 0, 0)$. Since the current source has only a time component, all internal currents must have only a time component in order to satisfy Kirchoff's laws. Where M is singular one must admit the existence of a real intermediate state, and the only ways of having such a state are as shown in Fig. 8, where particles $m_1, m_2 \cdots m_i$ are created at t_1 and propagate to t_2. It must be emphasized that this figure is to be taken as a literal picture--in coordinate space--of the intermediate state. Because of "Ohm's law", all currents, whose magnitudes are given by m_i, must propagate in the same direction, i.e. from t_1

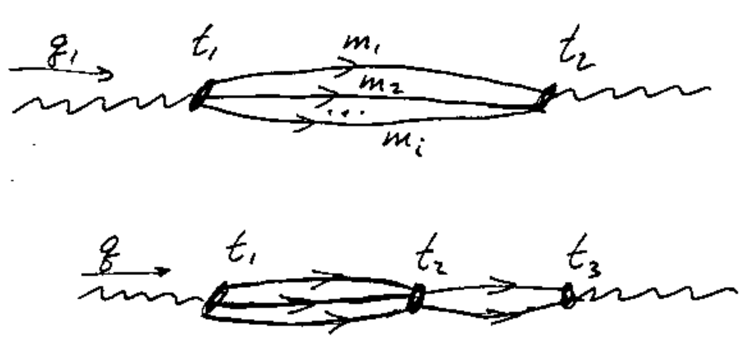

Figure 8: Typical singularities in the mass operator.

to t_2. We therefore have $q_o = \sum_i m_i$ at the threshold for singularities, where $\sum_i m_i$ is the minimum mass of the intermediate state.

VI. THE VERTEX FUNCTION

The vertex function Γ we shall study is that for which a quantum q decays into two particles of equal mass M.[13,14] It is straightforward but algebraically unpleasant to generalize this case. We consider Γ as a function of the momentum transfer q^2, which is to be extended into the complex plane. The kinematics are schematized in Fig. 9. It is easy to see that for $Re\, q^2 \leq 0$ Γ is analytic, i.e. the action J is negative definite. For if $q^2 = 0$, we may take $q_\mu \equiv 0$ for purposes of computing J. In this case, one sees that J is exactly the same as the J for the mass-operator for the particle of mass M, which indeed is negative definite at the value M^2, provided the particle M is stable. Since J is negative definite for $q^2 < 0$, it follows that all singularities of Γ must lie along the positive real q^2 axis. For positive q^2 we know that

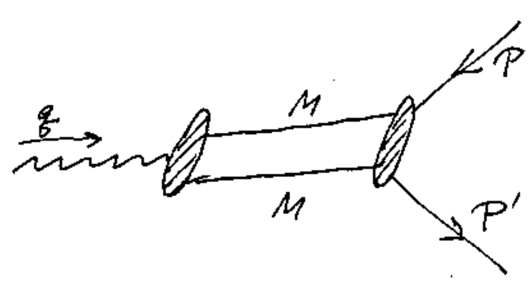

__Figure 9__: Singularity in the vertex function

J can vanish for $q^2 \geq 4M^2$, since in this case it is possible to have a real intermediate state of the two final particles as shown in Fig. 9. $q^2 \geq 4M^2$ defines the "physical region" in which the singularities are the obvious ones only.

The only region to investigate is that for which $0 \leq q^2 \leq 4M^2$. In this region it is convenient to choose the following coordinate system:

$$
\begin{aligned}
q_\mu &= (q, 0, 0, 0) \\
P_\mu &= \left(-\frac{q}{2}, i\sqrt{M^2 - \frac{q^2}{4}}, 0, 0\right) \qquad (27) \\
P'_\mu &= \left(+\frac{q}{2}, i\sqrt{M^2 - \frac{q^2}{4}}, 0, 0\right)
\end{aligned}
$$

Because of Kirchoff's laws all internal momenta must be of the form

$$k_\mu = (k_0, ik_1, 0, 0) \qquad (28)$$

where k_1 is real. For if there are no current sources in the 2-direction there cannot be any internal currents in the 2-direction. If the current sources in the 1-direction are all pure imaginary, all 1-components of the current in internal branches must be pure imaginary. Since all spatial momenta are pure imaginary, it is equivalent to real vectors in a Euclidean space; i.e. nothing is changed if we drop the i on the space components of the current and at the same time change the metric tensor from $g_{\mu\nu}$ to $\delta_{\mu\nu}$.

The existence of "real intermediate states" determines singularities in the vertex operator. Consider first the lowest order graph as shown in Fig. 10. Since all vectors involved are Euclidean and lie in a plane we may draw pictures in "coordinate space" in the sense of Ohm's law (1). Consider the possibility that all three intermediate particles can be simultaneously real. In this case the picture--illustrated in Fig. 10-- will be that the particle $\vec{P}$ dissociates at x_1 into particles $\vec{m}$ and $\vec{\mu}$ as shown. Since all particles involved are real, the angle θ is determined by momentum conservation: $2m\mu\cos\theta = M^2 - m^2 - \mu^2$. After $\vec{P}$ dissociates,

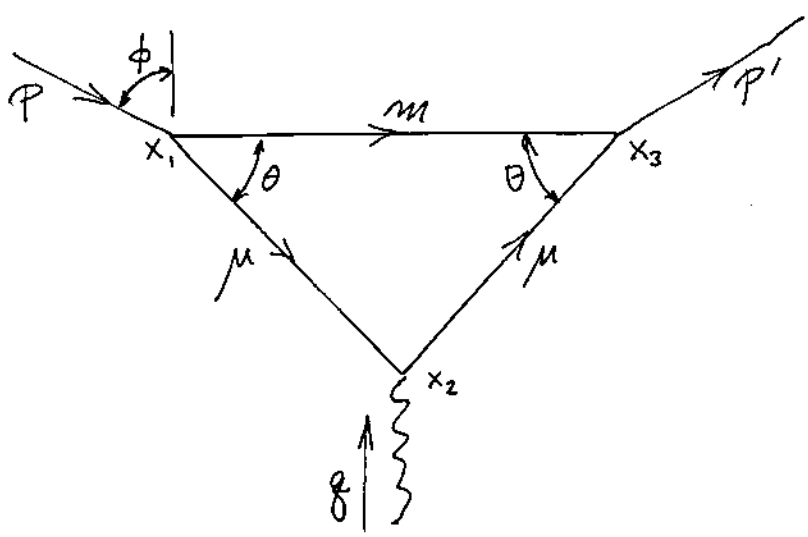

Figure 10: Lowest order graph for the vertex.

particle $\vec{m}$ must travel <u>to the right</u> because of Ohm's law. Particle $\vec{\mu}$ travels to x_2, where it scatters, and $\vec{m}$ and $\vec{\mu}$ recombine at x_3. The threshold occurs for $q = 2\mu \sin\theta$. In order for such a process to exist, θ must be less than $\frac{\pi}{2}$; if this is not true the line $\vec{m}$ must be short-circuited, and the diagram looks like Fig. 11 with a "normal" threshold of $q = 2\mu$. These pictures are readily generalized to higher orders. The main point is that if $\vec{P}$ dissociates at x_1, $\vec{q}$ is absorbed at x_2 and $\vec{P}'$ created at x_3, then all intermediate lines must lie inside the triangle (x_1, x_2, x_3). For assume the

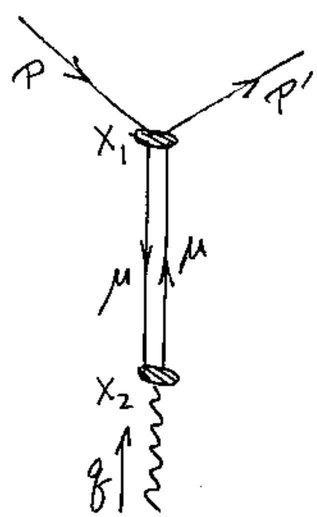

<u>Figure 11</u>: Singularity of vertex operator with normal threshold.

contrary, as in Fig. 12, and consider the point O. Because of Ohm's law, all the y-components of the current entering point O (from below) must be positive; however, it is then impossible to satisfy current conservation. Therefore such a situation cannot arise.

With this result it is possible to easily investigate the effect of higher order graphs. If it is impossible for particles $\vec{P}$ and $\vec{P}'$ to dissociate into a spray of lighter particles which subtend an angle of less than $\frac{\pi}{2}$, the one has only degenerate triangle intermediate states such as Fig. 11, and the threshold q_0 for singularities

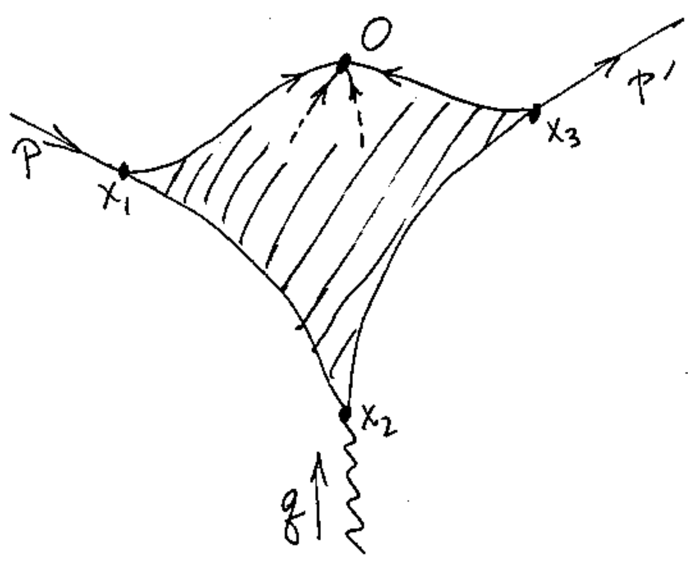

Figure 12: A situation for the vertex operator which cannot arise.

is just the lowest mass intermediate state. In the case of nondegenerate triangles the lowest threshold q_o is provided by the lowest order graph in cases of "practical" interest such as $\gamma \rightleftarrows D\bar{D}$ and $Y \rightleftarrows \Sigma\bar{\Sigma}$. One may be convinced after drawing a few of the possible pictures; a straightforward proof may be obtained in the "practical" cases since the angle θ can do nothing but increase and the angle 2ϕ between $\vec{P}$ and $\vec{P}'$ decrease as one considers higher orders. Both effects raise the threshold q_o.

The anomalous threshold occurs for weakly bound composite particles such as deuterons and for the hyperon electromagnetic vertex operators. In the case of the deuteron the angle θ is very small, and the threshold singularity occurs at $q_o \approx 4\sqrt{M\epsilon_B}$, where ϵ_B is the binding energy. An enumeration of the various thresholds will be found in reference 14. "Stable" particles such as nucleons, electrons, and pions have the normal threshold corresponding to the degenerate triangle.

VII. THE SCATTERING OF PARTICLES OF EQUAL MASS

In the case of scattering, our methods become somewhat less powerful. In order to keep the kinematical complications to a minimum, we shall only consider the case for which both particles have the same mass m. Let q_1 and q_2 be the incoming momenta and $-q_3$ and $-q_4$ the outgoing momenta. Then $\sigma^2 = (q_1 + q_2)^2$ is the square of the center-of-mass energy for the process, and $\bar{\sigma}^2 = (q_1 + q_3)^2$ and $\Delta^2 = (q_1 + q_4)^2$ are the corresponding quantities for the "crossed" processes. These quantities are related by the identity

$$\sigma^2 + \bar{\sigma}^2 + \Delta^2 = 4m^2 \qquad (29)$$

We shall attempt to describe all singularities of which are $o(\epsilon)$ from some real point (σ^2, $\bar{\sigma}^2$, Δ^2). There are three types of regions in the two-dimensional (σ^2, $\bar{\sigma}^2$, Δ^2) space, which are labeled A, B, and C in Fig. 13. In this figure we have used oblique coordinates in order to preserve the symmetry between σ^2, $\bar{\sigma}^2$, and Δ^2. The regions A are the physical regions for the reactions $1 + 2 \longrightarrow 3 + 4$, $1 + 3 \longrightarrow 2 + 4$, and $1 + 4 \longrightarrow 2 + 3$. The singularities in region A are only the obvious ones provided the scattering particles are stable. In region B,

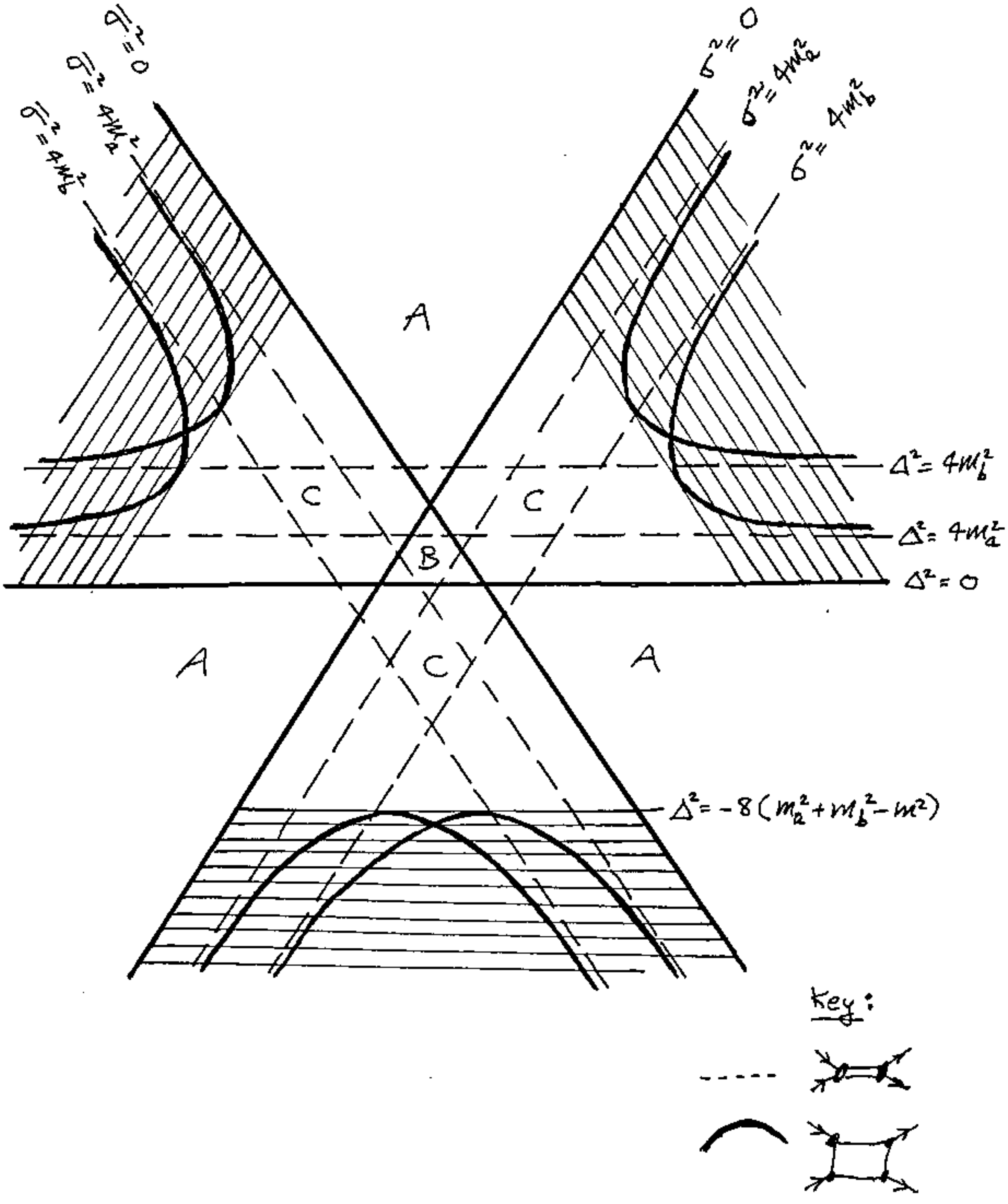

Figure 13: Singularities in the scattering of "very stable" particles. The key illustrates the type of singularity described.

$\sigma^2 > 0$, $\bar{\sigma}^2 > 0$, and $\Delta^2 > 0$, so that we may choose a coordinate system such that

$$q_1 = \left(\frac{\sigma}{2}, \frac{i\bar{\sigma}}{2}, \frac{i\Delta}{2}, 0\right) \qquad q_3 = \left(-\frac{\sigma}{2}, \frac{i\bar{\sigma}}{2}, -\frac{i\Delta}{2}, 0\right)$$

$$q_2 = \left(\frac{\sigma}{2}, -\frac{i\bar{\sigma}}{2}, -\frac{i\Delta}{2}, 0\right) \qquad q_4 = \left(-\frac{\sigma}{2}, -\frac{i\bar{\sigma}}{2}, \frac{i\Delta}{2}, 0\right) \qquad (30)$$

As in the case of the vertex operator, this choice allows the continuation into a Euclidean space, since all internal currents must be of the same form as the external currents. The determination of singularities is then completely analogous to the case of the vertex. For very stable particles such as nucleons, pions, or electrons, region B is free of singularities. To see this we replace the external q_i by λq_i and vary λ from 0 to 1. At $\lambda = 0$, J is clearly negative definite, and no singularities are encountered upon increasing λ from 0 to 1.

Those particles whose vertex function suffers anomalous singularities will also yield anomalous singularities in scattering processes. Some examples are illustrated in Fig. 14; a more complete enumeration appears in reference 14. In deuteron-deuteron scattering there exists no region where J is negative definite, so that even for forward scattering it is not possible with these methods to construct a dispersion relation.

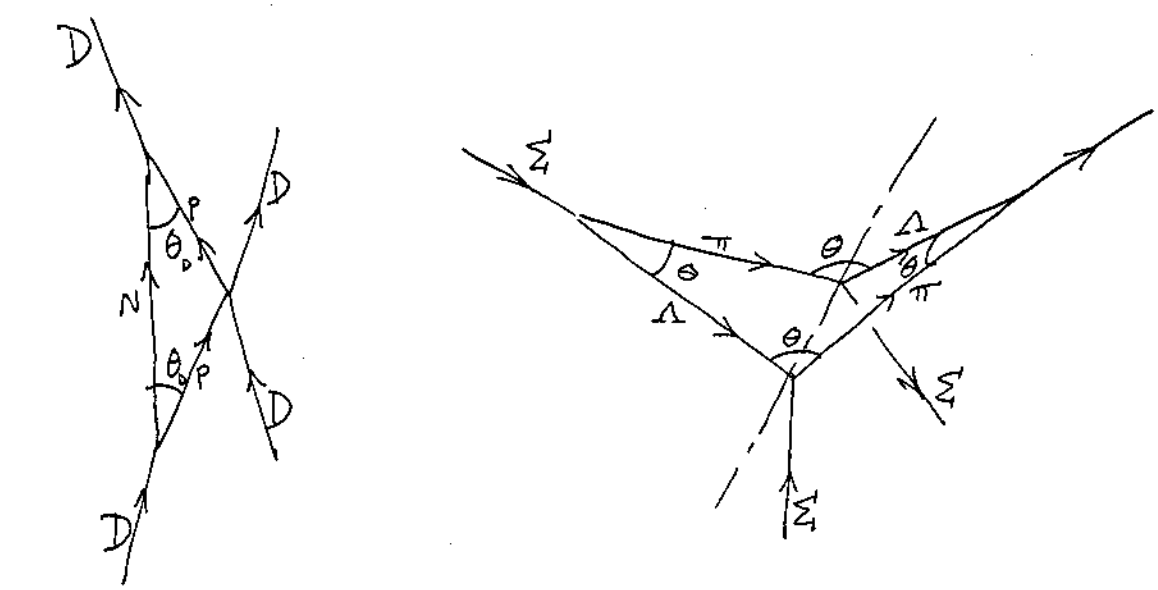

$$\cos\theta_D = \frac{M_D^2 - M_p^2 - M_N^2}{2M_p M_N}$$

(a)

$$\cos\theta = \frac{M_\Sigma^2 - M_\Lambda^2 - m_\pi^2}{2M_\Lambda m_\pi}$$

(b)

Figure 14: Anomalous singularities in scattering processes. All intermediate lines are real.

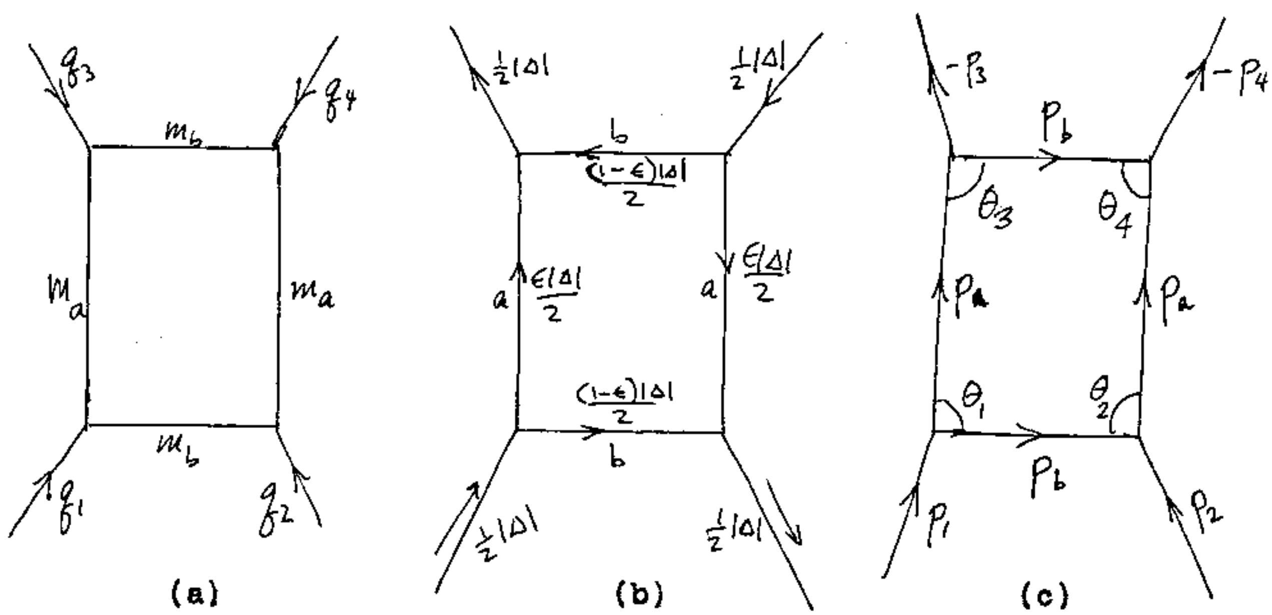

Figure 15: (a) Lowest order graph for scattering of equal mass particles.
(b) Circuit diagram in space-like dimension.
(c) Circuit diagram in time-like plane.

In region C, life is more unpleasant, and we shall be able to say rather little. In the region where $\sigma^2 > 0$, $\bar{\sigma}^2 > 0$, and $\Delta^2 < 0$ one may choose his coordinates so that

$$g_1 = \left(\frac{\sigma}{2}, \frac{i\bar{\sigma}}{2}, \frac{|\Delta|}{2}, 0\right) \qquad g_3 = \left(-\frac{\sigma}{2}, \frac{i\bar{\sigma}}{2}, -\frac{|\Delta|}{2}, 0\right)$$

$$g_2 = \left(\frac{\sigma}{2}, -\frac{i\bar{\sigma}}{2}, -\frac{|\Delta|}{2}, 0\right) \qquad g_4 = \left(-\frac{\sigma}{2}, -\frac{i\bar{\sigma}}{2}, \frac{|\Delta|}{2}, 0\right) \qquad (31)$$

We may then change to a metric for which $g_{\mu\nu} = (1,1,-1,-1)$

We first consider the lowest order graph shown in Fig. 15a. The only intermediate state whose threshold is not obvious from the previous discussion of the vertex function is that for which all four intermediate particles are real. We consider first the circuit equations in only the space-like dimension, illustrated in Fig. 15b. ϵ is yet to be determined. In the other two dimensions we may again make arguments similar to those for the vertex function. The picture in these two Euclidean dimensions is that of Fig. 15c, where the currents p_i, p_a, and p_b have magnitudes given by the equations

$$p_i^2 = m^2 + \frac{|\Delta|^2}{4} \qquad (i = 1,2,3,4)$$

$$p_a^2 = M_a^2 + \frac{\epsilon^2 |\Delta|^2}{4} \qquad (32)$$

$$p_b^2 = M_b^2 + \frac{(1-\epsilon)^2 |\Delta|^2}{4}$$

By straightforward geometry, one finds that all $\theta_i = \frac{\pi}{2}$, independent of ϵ. It then follows that

$$p_a^2 = \frac{\sigma^2}{4} \qquad p_b^2 = \frac{\bar{\sigma}^2}{4} \tag{33}$$

Upon eliminating ϵ, the condition for singularity is that

$$(\sigma^2 - 4m_a^2)(\bar{\sigma}^2 - 4m_b^2) = 4(m_a^2 + m_b^2 - m^2)^2 \tag{34}$$

provided $m^2 < m_a^2 + m_b^2$, which is just the condition that no anomalous singularities exist. We shall restrict ourselves hereafter to this case.

The minimum value of $|\Delta|^2$ for which there is a singularity described by (34) occurs when $\epsilon = \frac{1}{2}$, or

$$|\Delta_0^2| = 8(m_a^2 + m_b^2 - m^2) \tag{35}$$

If it is impossible for the external particles m to dissociate into a state containing particles m_i for which $\sum m_i^2 < m_a^2 + m_b^2$, then all other singularities of this nontrivial character must occur for $|\Delta|^2 \geq |\Delta_0^2|$. For consider what happens if we modify the graph into something like that of Fig. 16a. If $|\Delta^2| < |\Delta_0|^2$ the angle φ in Fig. 16c must be $> \frac{\pi}{2}$. For if it were not, we

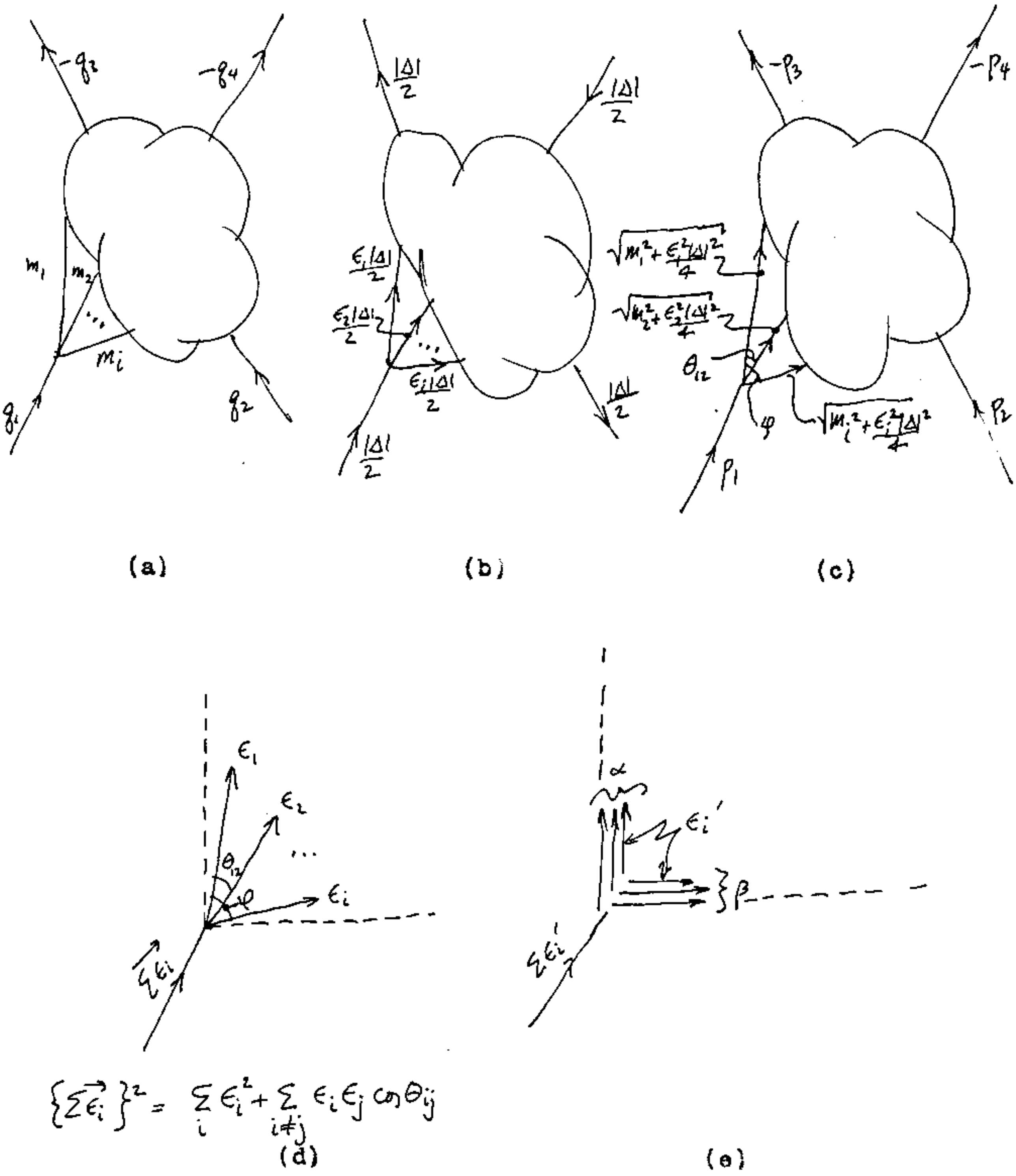

Figure 16: Higher order singularities in the scattering amplitude. (a), (b), and (c) are analogous to the diagrams in Fig. 15.

would have

$$m^2 + \frac{|\Delta|^2}{4} = \sum_i \left(m_i^2 + \frac{\epsilon_i^2|\Delta|^2}{4}\right) + \sum_{i\neq j} \sqrt{m_i^2 + \frac{\epsilon_i^2|\Delta|^2}{4}}\sqrt{m_j^2 + \frac{\epsilon_j^2|\Delta|^2}{4}}\cos\theta_{ij}$$

$$\geq \sum_i m_i^2 + \frac{|\Delta|^2}{4}\left\{\sum_i \epsilon_i^2 + \sum_{i\neq j} \epsilon_i\epsilon_j\cos\theta_{ij}\right\} \tag{36a}$$

But the quantity in brackets has the geometrical interpretation of Fig. 16d, and the angles θ_{ij} are identical to those of Fig. 16c. However one may now enclose the $\vec{\epsilon}_i$ by a right angle shown dotted in Fig. 16d and rotate each $\vec{\epsilon}_i$ over to one of the dotted lines in such a way that each time $\{\sum\vec{\epsilon}_i\}^2$ is decreased. The situation illustrated in Fig. 16e results and one has the result

$$\left\{\sum\vec{\epsilon}_i\right\}^2 \geq \left\{\sum\vec{\epsilon}_i{}'\right\}^2 = \left(\sum_\alpha \epsilon_\alpha\right)^2 + \left(\sum_\beta \epsilon_\beta\right)^2 \geq \frac{1}{2} \tag{36b}$$

since

$$\sum\epsilon_i = \sum_\alpha \epsilon_\alpha + \sum_\beta \epsilon_\beta = 1 \tag{36c}$$

We would then have

$$|\Delta|^2 \geq 8\left(\sum_i m_i^2 - m^2\right) \geq 8\left(m_a^2 + m_b^2 - m^2\right) \tag{37}$$

which contradicts the initial hypothesis.

We conclude that all singularities of this non-trivial character which are $o(\epsilon)$ of a real point $(\sigma^2, \bar{\sigma}^2, \Delta^2)$ are confined to the shaded regions in Fig. 13 provided the above-mentioned restrictions upon the mass spectrum are fulfilled. It is also clear from the requirements of Kirchoff's laws that the singularity in the shaded region corresponding to $\sigma^2 > 0$ and $\bar{\sigma}^2 > 0$ contributes only to the amplitude $\mathcal{M}_n$ (equation 23) corresponding to the "lumped circuit" illustrated in Fig. 6c.

We also speculate that the higher singularities are contained within the hyperbolae provided by the lowest order graph. However, the proof appears to be nontrivial.

Finally, we are able to say little concerning singularities in $\mathcal{M}$ when both σ^2 and $\bar{\sigma}^2$ are extended into the complex plane. The chief difficulty is that one can no longer use real resistors, since the contours in the z-integrations may be distorted into the complex plane. The geometrical methods we have used then lose their potency.

APPENDIX I: APPLICATIONS OF NETWORK THEORY

The method developed is of some practical usefulness in evaluating complicated Feynman diagrams, since with a little practice it is possible to write down the general solutions to a network by inspection of the graph. Borrowing some notions from network theory[17] we let a tree be any graph which connects all vertices but contains no closed loops. It is not uniquely defined. For a given tree, let the links be defined as the additional branches which must be added to the tree to complete the graph. If there are j links the current in any branch of the diagram is known if all external currents and all link currents are known. We consider the j link currents l_j as independent variables, which we shall denote as a link-basis. The loop through which the link current l_j flows may be uniquely defined

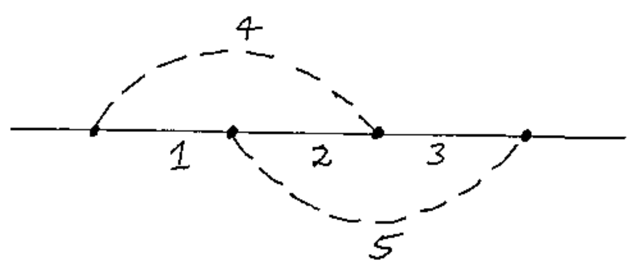

Figure 17: Illustration of trees and links. The solid line is a tree, and the dotted lines are links.

as that loop which remains when the other links are removed from the graph. Defining

$$\eta_{ij} = \begin{cases} \pm 1 \text{ if link current } l_j \text{ flows through } i^{th} \text{ branch} \\ 0 \text{ otherwise} \end{cases} \tag{38}$$

one may write Kirchoff's laws for the current k_i as

$$\left.\begin{aligned} \sum_i \eta_{ij} k_i z_i &= 0 \\ k_j &= l_j \end{aligned}\right\} \quad \text{for } j \text{ a link} \tag{39}$$

$$k_i = Q_i + \sum_j \eta_{ij} l_j \qquad \text{for } i \text{ in the tree}$$

Q_i is that sum of external currents q_i which flow through branch i if all links are removed. If one sets up (39) as a matrix equation for the n variables k_i

$$\sum_i A_{ki} k_i = Q_k \tag{40}$$

and solves them by Cramer's rule

$$k_i = \frac{K_i}{\Delta} \tag{41}$$

one finds, after staring at the determinants K_i and Δ, that they have the property that they are multilinear functions of the z_i; furthermore, $\frac{\partial K_i}{\partial z_i} = 0$. Δ, the network determinant, may be written down by inspection. It consists of a sum of products of j different resistances taken from the graph. A given product of z_i appears in $\triangle$ if, when removed from the graph, there is no open circuit, i.e. if the branches to which they refer form a link basis. If this is the case the coefficient of the product is +1. If this is not the case, the product does not appear in $\triangle$. For instance, the determinant corresponding to Fig. 17 is

$$\triangle = z_1(z_2 + z_3 + z_5) + z_2(z_3 + z_4 + z_5) + z_3 z_4 + z_4 z_5 \tag{42}$$

The fact that K_i is multilinear enables one to write it down by inspection also. We may write

$$k_i = \frac{K_i}{\triangle} = \frac{K_i^{\infty} z_1 + K_i^{0}}{\triangle^{\infty} z_1 + \triangle^{0}} \tag{43}$$

$\frac{K_i^{\infty}}{\triangle^{\infty}}$ will be the current in branch i when z_1 is removed from the graph; $\frac{K_i^{0}}{\triangle^{0}}$ will be the current in branch i when z_1 is short-circuited. By iterating this procedure, one can reduce the diagram to a trivial one.

Similar considerations hold for J. Because from (39)

$$\sum_i k_i^2 z_i = \sum_i Q_i \cdot k_i z_i \tag{44}$$

it follows that

$$J = \frac{\tilde{J}}{\triangle} - \sum_i m_i^2 z_i \tag{45}$$

where again $\tilde{J}$ is a multilinear function of the z_i. One may use the same reduction procedure to write down $\tilde{J}$ by inspection. The result for Fig. 17 is

$$\tilde{J} = k^2\left[z_2(z_1+z_5)(z_3+z_4) + z_1 z_4(z_3+z_5) + z_3 z_5(z_1+z_4)\right] \tag{46}$$

Thus any network quantity may readily calculated by this procedure.

APPENDIX II: RULES FOR FEYNMAN DIAGRAMS

We are now able to study in more detail the quantity $N(q_i, z_i)$ defined in Chapter III. We may write

$$N(q_i,z_i) = \left(\frac{-i}{2}\right)^m \int d^4l_1 \cdots d^4l_j \, e^{\frac{i}{2}\sum_i L_i^2 z_i} \, e^{i\sum_i L_i \cdot x_i} \, M(k_i, q_i) \, \delta^{(4)}(\Sigma q_i) \quad (47)$$

The integrations range over all link variables l_j. L_i is the current in the i^{th} branch when all external currents q_i are turned off and link currents l_j turned on; i.e. $L_i = \sum_j \eta_{ij} l_j$. $x_i = \frac{1}{i}\frac{\partial}{\partial k_i}$ is a displacement operator. The integration is now of a standard Gaussian type; introducing

$$Z_{jk} = \sum_i \eta_{ij} \eta_{ik} z_i = Z_{kj} \quad (48)$$

one may write

$$N(q_i,z_i) = \left(\frac{-i}{2}\right)^m \int d^4l_1 \cdots d^4l_j \, e^{+\frac{i}{2}\sum_{jk} l_j \cdot l_k Z_{jk}} \, e^{i\sum_{ij} \eta_{ij} l_j x_i} \, M(k_i, q_i) \, \delta^{(4)}(\Sigma q_i) \quad (49)$$

If one diagonalizes Z_{jk} with a unitary matrix and shifts the origin of coordinates, the integrals may be carried out, and one obtains

$$N(q_i,z_i) = \left(\frac{-i}{2}\right)^m \frac{(-4\pi^2 i)^j}{\Delta^2} \, e^{-\frac{i}{2}K} \, M(k_i, q_i) \, \delta^{(4)}(\Sigma q_i) \quad (50)$$

where

$$K = \sum_{ijkl} x_i \eta_{ij} x_k \eta_{kl} G_{jl} \tag{51}$$

G_{jl} is the inverse of Z_{jk} and $\Delta = \det Z$. It is the same Δ which we have encountered previously. The displacement operator K has a fairly simple interpretation. We turn off the external currents q_i and turn on in each link current sources l_j. Let X_j be the voltage directly across the link source l_j, and make the identification

$$X_j = \sum_i x_i \eta_{ij} = \sum_{ik} (\eta_{ik} l_k z_i) \eta_{ij} = \sum_k Z_{jk} l_k \tag{52}$$

We see that the power burned up in such an arrangement is

$$K = \sum_j X_j \cdot l_j = \sum_{kj} X_k G_{kj} X_j \tag{53}$$

K is the power burned up in a circuit in which voltage sources X_j are placed in all links, such as in Fig. 18.

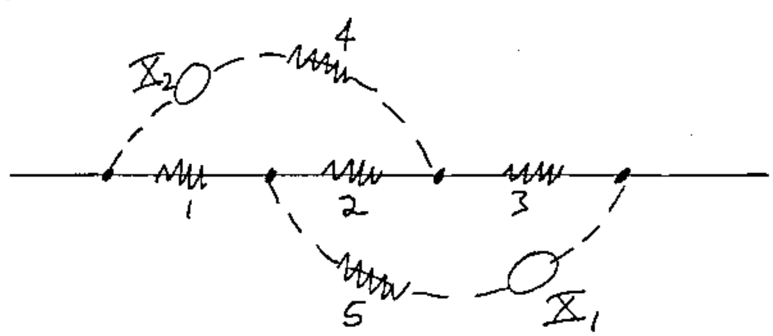

Figure 18: Graph illustrating computation of the displacement operator K.

It is a ratio of two multilinear functions of the z_i, with the network determinant Δ as denominator, so that with a little practice it may be written down by inspection by means of the reduction procedure outlined in Appendix I. The rule for computing K is to first remove j-1 resistors z_κ from the graph. If there is a loop left over write down

$$\prod_{\alpha=1}^{j-1} z_\alpha \Big(\sum_{loop} x_i\Big)^2 \tag{54}$$

Otherwise write down nothing. Do this for all combinations of j-1 resistors. To obtain K add up all the contributions and divide by Δ.

We then have a complete prescription for writing down the contribution of a given Feynman diagram in parameter form. It is given by

$$\mathcal{M}(q_i) = (-4\pi^2 i)^j \left(\frac{-i}{2}\right)^n \int \frac{d^n z}{\Delta^2} e^{\frac{i}{2}J} e^{-\frac{i}{2}K} M(k_i, q_i)\,\delta^{(4)}(\Sigma q_i) \tag{55}$$

One expands the exponential in order to perform the differentiations upon M, which is defined in (9).

APPENDIX III: MISCELLANEOUS THEOREMS

<u>Theorem 1</u>: The action function J is expressible in the form

$$J = \frac{1}{2}\left[\sum_\alpha \rho_\alpha Q_\alpha^2 - \sum_i m_i^2 z_i\right] \qquad (56)$$

where the parameters ρ_α are positive.

The proof follows from the iteration procedure outlined in Appendix I. Since

$$J = \frac{1}{2}\left[\frac{z_1 J^\infty + J^\circ}{z_1 \Delta^\infty + \Delta^\circ} - \sum_i m_i^2 z_i\right] \qquad (57)$$

and J^∞/Δ^∞ and J°/Δ° are the power burned up in a simpler circuit, we see that after n iterations we are led to a sum of terms with positive coefficients composed of products of z_i and a $1/\Delta$. Each term will be the power burned up in a tree which results from removing j resistors from the diagram and clearly is of the form $\sum_\alpha Q_\alpha^2 z_\alpha$. Hence the complete J must have the structure indicated in the statement of the theorem.

<u>Theorem 2</u>: The statement of this theorem appears in Chapter V.

The analyticity properties of $\mathcal{M}$ are the same as

$$\mathcal{M}' = \int_0^\infty \frac{dz_1 \cdots dz_n \, \Phi(z_1 \cdots z_n)}{\Delta^2 [J + i\epsilon]^m} = \int_0^\infty dz_1 \cdots dz_n \, f_1(z_1 \cdots z_n, Q_1^2 \cdots Q_\alpha^2) \tag{58}$$

We do not choose Φ a δ-function, but rather some function such as $\Phi = (\Sigma z_i)\, e^{-(\Sigma z_i)}$ so that we are not bothered by a constrained region of integration. f_1 has the property that, for $\epsilon > 0$, it is analytic for all real values of the parameters z_1 and Q_α^2. Furthermore f_1 may be extended into the complex planes of any of the z_1 and Q_α^2 by a distance $o(\epsilon)$ because of the stationary property of J; that is if $z_i \to z_i + i\delta z_i$, $Q_\alpha^2 \to Q_\alpha^2 + i\delta Q_\alpha^2$

$$J + i\epsilon \to J + i\Sigma(k_i^2 - m_i^2)\delta z_i + i\sum_\alpha \xi_\alpha \delta Q_\alpha^2 + i\epsilon \tag{59}$$

A necessary condition for a singularity of f_1 is that $J(z_1 \cdots z_n, Q_1^2 \cdots Q_\alpha^2) = 0$. In order that $\mathcal{I}m\, J = 0$, the δz_1 and δQ_α^2 must be $o(\epsilon)$. We now consider

$$f_2(z_2 \cdots z_n, Q_1^2 \cdots Q_\alpha^2) = \int_0^\infty f_1(z_1 \cdots z_n, Q_1^2 \cdots Q_\alpha^2)\, dz_1 \tag{60}$$

f_2 is a well-defined integral for real z_1 and Q_α^2 , and it is analytic in the neighborhood of any real point. f_2 can be singular $o(\epsilon)$ only if, as $\epsilon \to 0$, the integral is not well-defined. This can happen only if, as illustrated in Fig. 19, two singularities coincide (A) or if a singularity occurs at $z_1 = 0$ (B) . Isolated singularities (C), including branch points, cannot produce a singularity in f_2, since the integration contour may be deformed away from the singularity and f_2 remains well defined as $\epsilon \to 0$.

Hence, a necessary condition for a singularity $o(\epsilon)$ in f_2 is that either

$$\begin{aligned} &(a) \quad J = 0 \quad \text{and} \quad \frac{\partial J}{\partial z_1} = 0 \\ &(b) \quad J = 0 \quad \text{and} \quad z_1 = 0 \end{aligned} \tag{61}$$

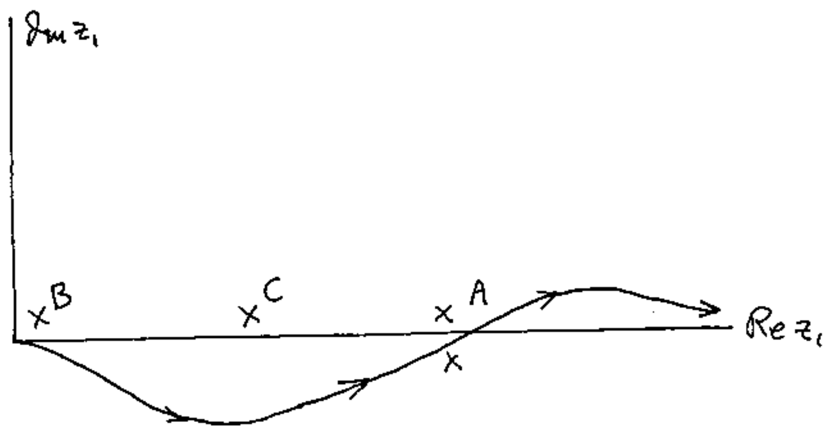

Figure 19: Integration over a resistance parameter.

We may use the right hand equation to eliminate z_1, so that $J(z_1, z_2 \cdots z_n, Q_\alpha^2) = 0$ expresses the condition on z_2 for a singularity. We continue the process and consider

$$f_3(z_3 \cdots z_n, Q_1^2 \cdots Q_\alpha^2) = \int_0^\infty dz_2\, f_2(z_2 \cdots z_n, Q_1^2 \cdots Q_\alpha^2) \tag{62}$$

f_3 can be singular only if (c) f_2 has two singularities $o(\in)$ of each other and of the real positive z_2 axis or if (d) f_2 is singular at $z_2 = 0$. In case (c) one must have

$$J = 0 \qquad \text{and} \qquad \frac{\partial J}{\partial z_1}\frac{\partial z_1}{\partial z_2} + \frac{\partial J}{\partial z_2} = \frac{dJ}{dz_2} = 0 \tag{63}$$

Because of (62) the left hand term vanishes and the condition for a singularity in f_3 is that

$$J = 0 \quad \text{and either} \quad \left\{ \begin{array}{c} \dfrac{\partial J}{\partial z_i} = 0 \\ z_i = 0 \end{array} \right\} (i = 1,2) \tag{64}$$

The proof then follows by induction.